2003

Impacts to dispersion and variance of species in microflows involving turns

Sean Matheson
San Jose State University

IMPACTS TO DISPERSION AND VARIANCE OF SPECIES IN MICROFLOWS INVOLVING TURNS

A Thesis

Presented to

The Faculty of Department of Mechanical and Aerospace Engineering

San Jose State University

In Partial Fulfillment

of the Requirements for the Degree

Master of Science

by

Sean Matheson

August 2003

INFORMATION TO USERS

The quality of this reproduction is dependent upon the quality of the copy submitted. Broken or indistinct print, colored or poor quality illustrations and photographs, print bleed-through, substandard margins, and improper alignment can adversely affect reproduction.

In the unlikely event that the author did not send a complete manuscript and there are missing pages, these will be noted. Also, if unauthorized copyright material had to be removed, a note will indicate the deletion.

ProQuest Information and Learning Company
300 North Zeeb Road
P.O. Box 1346
Ann Arbor, MI 48106-1346

APPROVED FOR THE DEPARTMENT OF MECHANICAL AND AEROSPACE ENGINEERING

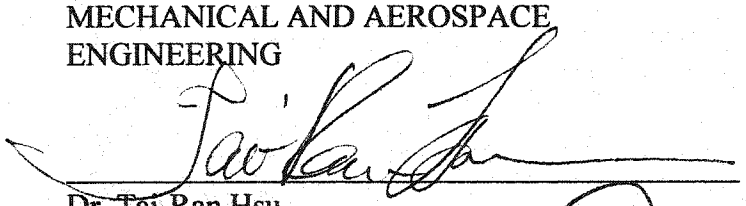

Dr. Tai-Ran Hsu

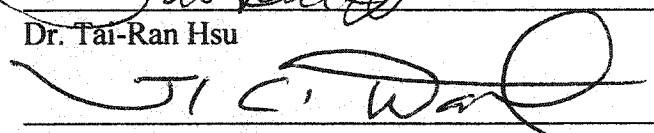

Dr. Ji Wang

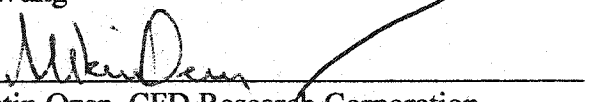

Dr. Metin Ozen, CFD Research Corporation

APPROVED FOR THE UNIVERSITY

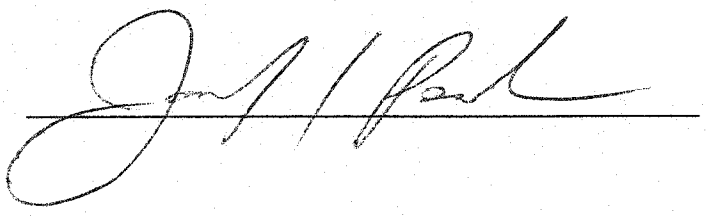

ABSTRACT

IMPACTS TO DISPERSION AND VARIANCE OF
SPECIES IN MICROFLOWS INVOLVING TURNS

by Sean Matheson

Three techniques are studied to understand the impact on a sample after it traverses a turn using simulations from CFD-ACE+ and historical results. Plain turn studies are compared with results from an assumed linear electroosmotic flow profile across the channel and with a simulated step change in potential. Results show that CFD-ACE+ results are similar to previous studies and useful for modeling complicated transient scenarios. For the plain turn studies with small radii, CFD-ACE+ results show similar results to historical studies at high modified Peclet numbers, with a shift of the sample to the inner edge of the turn. For electroosmotic flow change, at high Peclet number, dispersion is correctable over short distances, with error of 10-20% for experimental and 4% for simulated results. A step change in potential adversely affects dispersion, but variance is beneficially affected. Recommendations for channel design are discussed, with a summary given.

Acknowledgements

I would like to thank my thesis advisors for being so patient, as it has been almost a year that I have worked on this thesis, and another year beyond the first year that I had been preparing to start work on it.

I would like to thank Dr. Metin Ozen, for the use of the wonderful software used in the simulations and the computers at the CFDRC office. I can think of thousands of uses for the software, but I simply just didn't have the time to run all the scenarios.

I would like to thank Dr. Tai-Ran Hsu, who has been extremely helpful with guiding me toward the topic, as I have a tendency to pick large projects and sometimes have difficulty narrowing them down to more manageable pieces.

I would like to thank Dr. Ji Wang, who has been a wonderful teacher for the large number of control-related courses I have taken at San Jose State University. The amount of work put into the courses has left me with a feel for systems theory that I have applied in numerous engineering areas.

Finally, I would like to thank my parents for giving me the determination to succeed in spite of the numerous setbacks I have had over the last six years. Without it I would not have finished this and hope that it will continue to be an asset that I can rely on in the future.

Table of Contents

List of Figures

List of Tables

List of Nomenclature (in Order of Appearance)

c	Concentration of species, J.
J	Flux of concentration through area, A.
t, T	Time.
x, X	X-Dimension.
D, D_i, Γ, Γ_e	Diffusion constant of a species, diffusion constant of the ith species, diffusion constant of a species, and diffusion constant of the eth species.
$\vec{V}$ $\vec{u}$	Velocity of a species
ϕ, Φ, V	Electric potential.
y, y_j	Y-Dimension, jth dimension in a dimensional space.
$\lambda_D, 1/\kappa$	Debye-Huckel length.
ζ	Zeta potential.
c_0	Ion concentration balance point.
Φ_w	Electric potential at surface of channel.
ρ	Density of a fluid.
τ_{ij}	Fluid stress tensor, i and j are indices.
$\vec{g}$	Gravity vector.
ρ_E	Density of electrons in a fluid.
$\vec{E}$, E_x	Electric field, electric field in x direction.
μ, υ	Dynamic viscosity of a fluid.
ε	Permitivitty of free space.
U	Speed of a fluid.
μ_{eo}	Electroosmotic mobility.
z_i	Charge of ion on a species, i.
μ_{ep}, ω_i	Electrophoretic mobility of a species, electrophoretic mobility of species, i.
$\vec{v}$	Velocity of a fluid.
S_{Mx}, S_{Mx}	Sum of miscellaneous force terms in x, y directions.
p	Pressure acting on fluid.
π	Ratio of circumference of circle to diameter.
A, A_e	Area of a plane or surface of a side of a cell.
υ	Control volume of a cell.

$\vec{n}$ ---------- Normal unit vector from a cell surface.

C_e ---------- Mass flux across a cell surface.

$\vec{e}$ ---------- Vector of cell 'P' to cell 'E'.

δ ---------- Distance between centers of cells, also width-radius ratio.

$\vec{\tau}$ ---------- Vector defined by C1, C2 cells.

r ---------- Radius of turn.

a,w ---------- Width of turn.

Re ---------- Reynolds number.

Pe ---------- Peclet number.

σ ---------- Standard deviation.

σ^2 ---------- Variance.

θ ---------- Arc length of turn in radians.

t_d ---------- Diffusion equilibrium time.

t_t ---------- Turn travel time.

v_c ---------- Speed at center of channel.

r_c ---------- Radius at center of channel.

F ---------- Ratio of upper to lower channel electroosmotic velocity.

CFL---------- Courant, Friedrichs, and Lewy number.

δPe ---------- Modified Peclet number.

$(\sigma/a)^2$ ---------- Normalized variance.

$(\sigma/2\theta w)^2$ ---------- Scaled variance.

t_d/t_t ---------- Time ratio.

H ---------- Plate height.

D_{eff} ---------- Effective diffusion constant.

u_{eo} ---------- Electroosmotic velocity.

h ---------- Height of channel.

1.0 Introduction

Microfluidics and micromechanical systems (MEMS), with applications in the biotechnology industry, have had a significant amount of research applied to them recently. Of particular interest is the concept of the lab-on-a-chip, which over the last 10 years has had a nearly exponentially increasing amount of research. This lab-on-a-chip concept has driven research into chips that separate samples, and over the last few years this research has been narrowed down to making the separation process quicker, more efficient, more manufacturable, and with less waste than the larger systems that are available on the market today. The most common separation technique researched recently in these chips has been with electrokinetics. This separation technique, first originating from capillary electrophoresis (CE), is ideal for miniaturization as there are no moving parts. The study here is limited to one aspect of the design of the chip, as the design of a complete device is far too broad a topic to cover in a single paper. The design aspect of interest here is how the sample traverses the turn. Diverting a sample 90 or 180 degrees through a turn adversely distorts a sample moving in a planar fashion such that one side of the sample near a channel wall will lead the side of the sample at the opposite wall. This phenomenon is associated with the term dispersion and detection of individual species in a sample becomes more difficult when the species are very similar, as the normally separated distance between two species may be shorter than the actual dispersion length. The variance of a sample from a planar profile is calculated as statistical variance, and is normally affected only by the diffusion constant and time for each individual species. Dispersion tends to "widen" the sample, thus variance is also

adversely affected by the turn, as variance is normally determined in a one-dimensional manner. For these reasons, detection of individual species in a sample becomes challenging as the sample is distorted to appear wider than it normally is when looked at in a one-dimensional manner. Recently, several studies have investigated this problem experimentally and analytically, but under limited conditions. This thesis integrates much of the information from the current literature, and compares different methods through analytical, experimental, and simulated results in comparing the impact to dispersion and variance after a species travels a turn.

This study begins with the scope of the thesis and an introduction to capillary electrophoresis. It then expands to the more recent studies of electrophoresis on the micron scale, including the importance of turns on small-scale geometries. The next section details the general physics relating to the geometry, and then the numerical modeling parameters of a proprietary software program used to complement the results from the current literature are discussed. Next, the initial conditions, comparison criteria, and calculations for analysis specific to this problem are discussed. The results from the verification studies, simulations, experiments, and literature are then presented in the results section. The results of the simulations, analytical results, and experiments are discussed, and finally the conclusions of this thesis are presented.

The main interest in turns is from a desire to maximize space, and to begin to develop a "toolbox" for use in more complex geometries. Separation using electrokinetics requires a long channel or tube to separate the sample into multiple species. Typical separation times are of the order of 200 seconds and separation lengths

of 1-2 meters for CE systems are common. Thus for miniaturization, some method to optimize the area that a device occupies is necessary. Systems have been designed with small angle turns, and several separation channels with one sensor to increase throughput. Some systems are simply one channel with numerous tight turns to minimize the space required. There are numerous other designs for separation devices, all of which are specific to the particular application and specifications.

In Figure 1, two different separation system designs are shown, one without turns (top), and one with turns (bottom). The typical separation control sequence is to first

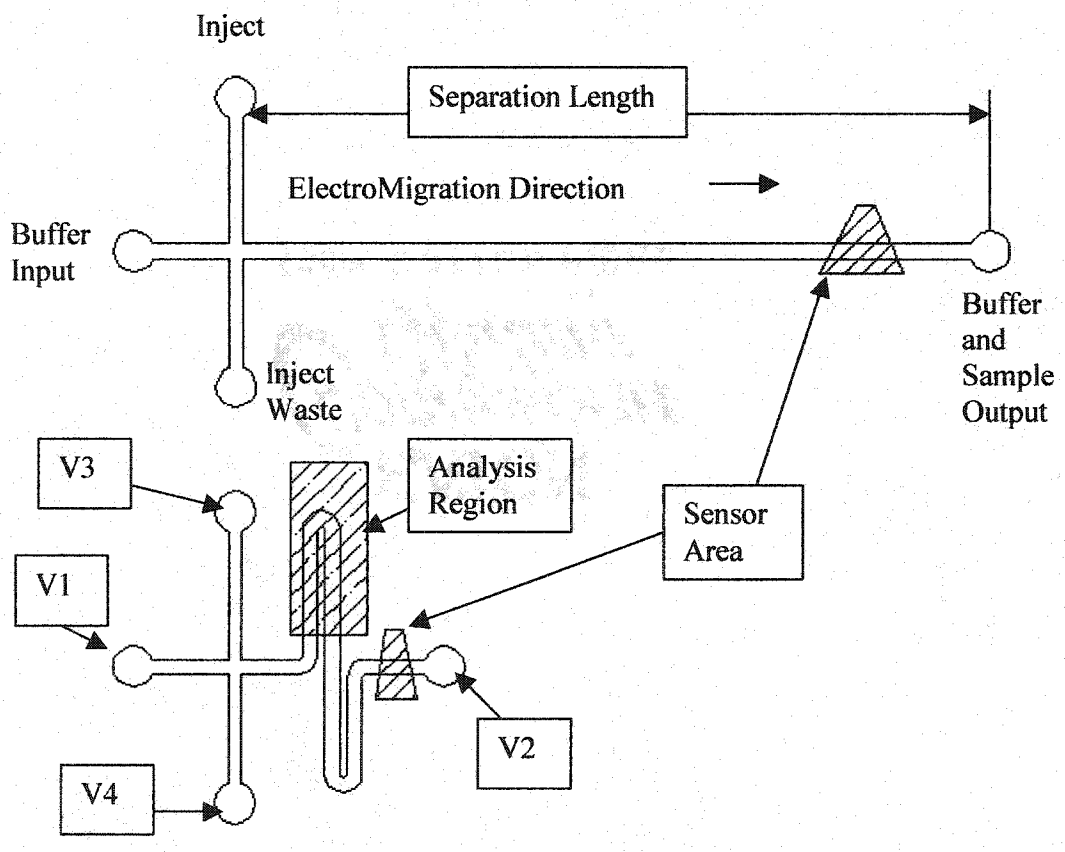

Figure 1: Diagram of Typical Microfluidic System (With Turns, Without Turns).

flush the separation channel system with a buffer fluid (indicated as buffer input-buffer and sample output in Figure 1), and then inject a sample with a species to be analyzed (inject-inject waste) until the sample is in the cross junction. Next, an electric field is applied between the buffer input and "buffer and sample output" position to drive the sample toward the sensor area. The difference between the two designs in the figure is the number of "systems" that can be constructed on a single plate, which would then be broken up and made into different individual devices later. As can be seen in Figure 1, at least two systems could be constructed in the same area with turns as a system without turns. A constant radius turn or even a sharp corner is the preferred design, as this geometry is easier to manufacture. This is not necessarily always true as a 'standard' manufacturing method has not been defined, but from a design standpoint a constant radius design is simpler to design over a complex spline.

There are other reasons for studying this problem, such as the three dimensional effects of how the species travels a turn or a corner when the electric field is multi-dimensional. Studying these methods will give some idea of how the phenomenon of electroosmotic flow will affect the flow of fluid in the micron scale for use in other applications such as electroosmotic pumping of fluid.

1.1 Scope

The focus of this thesis is limited to understanding the impact of three methods on the variance and dispersion of a sample after a turn in various configurations on the micron scale. Variance of a sample, normally affected only by time and diffusion constant, is extended as dispersion makes the sample seem wider when observed in a one-

dimensional manner. Dispersion, normally not affected at all, is generated as one side of the sample appears to move faster than the other side through path length differences in the inner and outer radius of the turn and from differing electric field strengths. The turns studied have constant width and radius cross-section for a simple analysis. The comparison criteria used are the variance and the dispersion of the species across the channel, as discussed in recent literature. The methods studied are an electroosmotic flow change from opposite sides of the channel after the turn, a constant electric field timed to change in the turn, and the plain turn design, for comparison. Current literature and experimental results are used to compare the analytical, experimental, and simulated methods.

1.2 History of Capillary Electrophoresis

Studies of electrokinetics originate from the pioneering work done by Michael Faraday in 1833-1834, who studied and generated the standard laws of electrolysis. This was followed by studies done by Hittorf, Hemholtz, and Kohlrauch for the remainder of the 19th century, who separated electrokinetics into ionic mobility (electrophoresis) and bulk mobility (electroosmosis) and made some basic formulations of how the electrophoretic mobility of a species is related to the ionic radii (Camilleri, 1998).

Tiselius was one of the first to study electrophoresis of proteins, and was able to determine that their mobilities were dependant on the molecular weight. Later he discovered the problems with the temperature effects of diffusion at high electric field strengths, known as Joule heating, and resolved this by circulating water around the medium to remove the heat to reduce the diffusion. Here Tiselius experimented with

paper, rather than capillary electrophoresis (CE), which has grown in popularity in the last 10 to 20 years (Camilleri, 1998).

Tiselius then progressed to paper and gel electrophoresis, a method used widely by scientists up until 10 to 20 years ago, and is still in use today, although simpler methods are used now. Paper and gel electrophoresis are two common CE techniques that have been successful in the resolution of ionized compounds of relatively small molecular weight and have relatively good resolution with small quantities of analyte. This method involves applying the analyte to special filter paper, and applying a voltage across the paper, of the order of 100 V/cm. From these studies, many of the common methods of electrophoresis, such as isoelectric focusing, have been established (Camilleri, 1998).

Capillary electrophoresis has had much interest in it over the last 5 to 20 years from simplicity and high reproducibility. The difficulty with using a gel or filter paper is that the paper is a consumable, and it is difficult to automate testing multiple species. In capillary electrophoresis, the sample is injected into the capillary using a syringe pump or siphoning, and can be automated easily using current technology. Diffusion from joule heating can be reduced as a thin wall capillary can dissipate heat faster in high electric field cases. Most of the various methods of electrokinetics separation established by the original pioneers can also be used with a capillary tube, another advantage to CE. In common practice capillary diameters of 300 to 500 microns or less are used for CE applications. In CE practiced with smaller capillaries of 300 micron or less there are fewer convection problems and very efficient electrophoretic separations compared to

larger diameter capillaries. The details of the various separation methods are quite involved and only one is discussed here, open tubular, or capillary zone electrophoresis (Camilleri, 1998).

Detection instrumentation used in CE is typically a UV detector with an electromagnetic wavelength selection from 190 to 700 nm. Other methods of detection include fluorescence, mass spectroscopy, Raman, amperometry, conductivity and radiochemical methods (Camilleri, 1998). Each method is unique to the molecule being analyzed, and is one of the challenges of designing a generalized lab-on-a-chip device.

1.3 History of Microfluidics

Much of the recent research in miniturization of separation systems is linked with research done by Andreas Manz. The researcher wrote a paper which is cited extensively in recent literature in various forms. The paper, titled: 'Planar Chips Technology for Miniaturization of Separation Systems: A Developing Perspective in Chemical Monitoring', summarizes some of the recent advances of miniaturization in the decade up to 1993. In the paper, the acronym μ-TAS was used to describe 'Micro-Total Analysis Systems' instead of the more current MEMS (Micro Electro Mechanical Systems). The studies include a planar CE device, where the channel spirals toward the center of the device, as fabricated by Hitachi in 1990. Various pumps, valves, and chemical actuation methods are also discussed, and simplified equations at the micron scale are summarized in the paper (Manz, 1993).

1.4 Recent Studies: Research in Turns

The first study that was conducted on turns was by a group from Oak Ridge National Laboratory in 1998. The authors developed a set of equations based on the electric field and geometry and compared the predicted results of these equations to experimental data they obtained through testing three cases. The results obtained from the experimental results closely matched the equations developed in the paper. The most important discovery of the study was that the control of dispersion in the turns can be made by adjusting the t_D/t_t ratio, defined as the ratio of the transverse diffusion equilibrium time (t_D) to the time spent in the turn (t_t). This will be further discussed in the results section (Culbertson, Jacobson, & Ramsey, 1998).

The next group of researchers experimented with a variety of channels with different width-radius ratios, a square turn design, and a design which was tapered just before the turn. The results showed that a second turn after the first turn removes some of the dispersion from the first turn. The tapered channels with wide channel widths outside of the turn, and narrow width channels inside of the turn minimized dispersion while maximizing the separation efficiency of the system. The advantage of the tapered design is a reduction in the extreme levels of dispersion in the region when the width is small compared to the radius (Paegel, 2000).

The next two studies involved numerical modeling of the U-shaped turn using a Monte Carlo simulation method. A group of people working at Sandia National Laboratories modeled the physics of the problem using a simplified form of the Navier-Stokes equations, using Poisson's equation to determine the electric field around the turn.

The electroosmotic mobility (EOM) and electrophoretic mobility (EPM) were assumed similar phenomenon for the study, with the response of the fluid to these mobilities as being linear in nature. The variables were dimensionally normalized to reduce the number of independent variables. They discovered what some of the experimentalists had already understood, that the primary effects of dispersion were dependant on the width-radius ratio, and that at large ratios (small radius) there was a significant amount of additional variance. This study only considered the problem from the point of the dispersion of the turn, and described the variance from the dispersion of the band around the turn as a square profile. A normal distribution across the channel was found to be dependant on the width-radius ratio, with no explanation given (Griffiths & Nilson, 2000).

1.5 Recent Studies: Material Change after a Turn

In addition to changes of geometry to adjust the profile of the sample as it leaves the turn, material changes to the channel walls have been suggested and experimentally tested. The purpose was to slow down the flow at one side of the channel so that the trailing edge can catch up with the other side (or speed up the flow on one side). Only one study has been done in this area, with a group of scientists at the National Institute of Standards and Technology (NIST) who changed the zeta potential on one side of the turn to speed up the flow in that area. In 2001, this group modified a 90 degree turn so that the inside channel had a different charge than the outside of the channel, as shown in Figure 2. In the study, UV light was used to modify the surface charge of the wall in poly(methyl methacrylate). The EOM increased by 4 percent for areas of excited regions

versus the non-excited regions. The group also noticed a reduction in plate height (similar to variance) by approximately 40 percent in a 90-degree turn for the modified

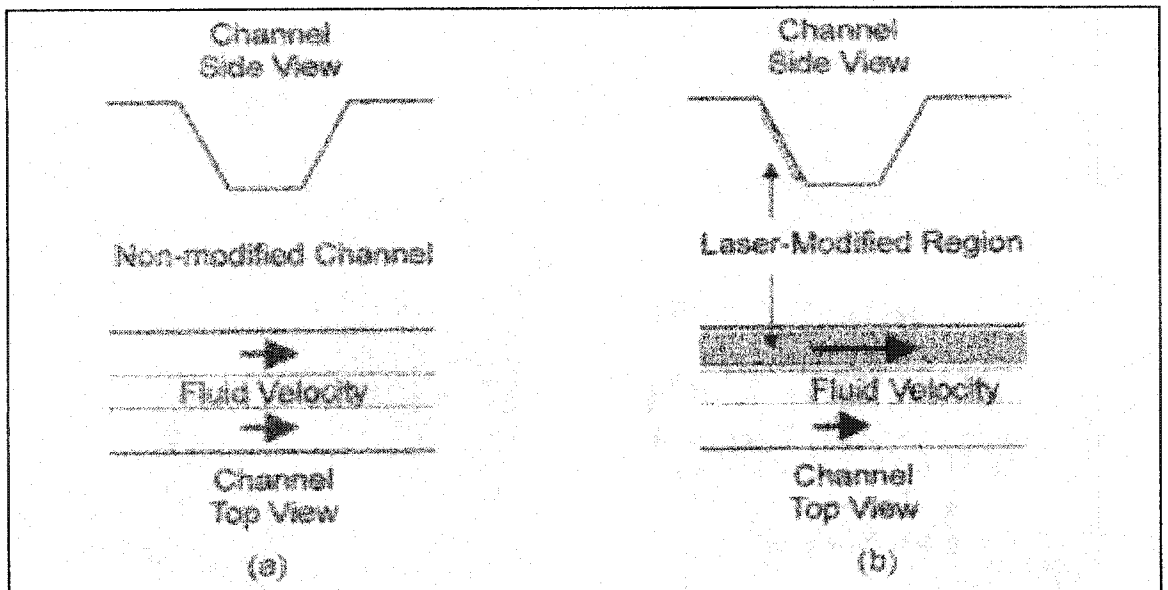

Figure 2: Cross-Section of Trapezoidal Channel (Johnson et al., 2001).

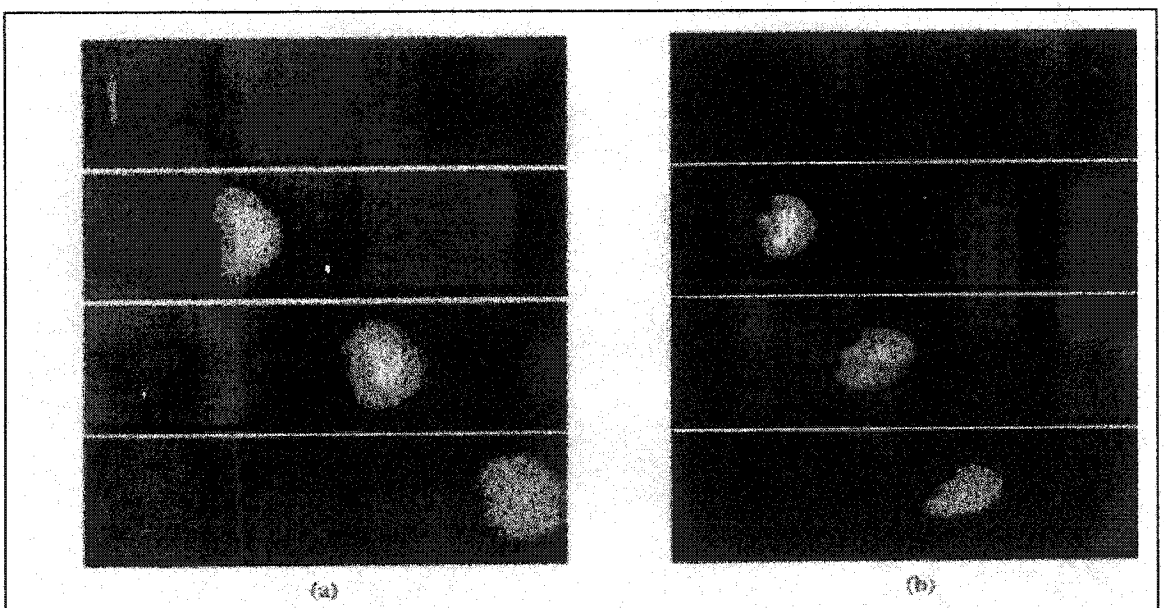

Figure 3: Images of a Species in Unmodified (a) and UV-Modified (b) Channels (Johnson et al., 2001).

turn versus the unmodified turn for four different average velocities. The group also studied the effects of a single band traveling straight, as shown in Figure 3 and 4 (Johnson, Ross, & Locascia, 2001).

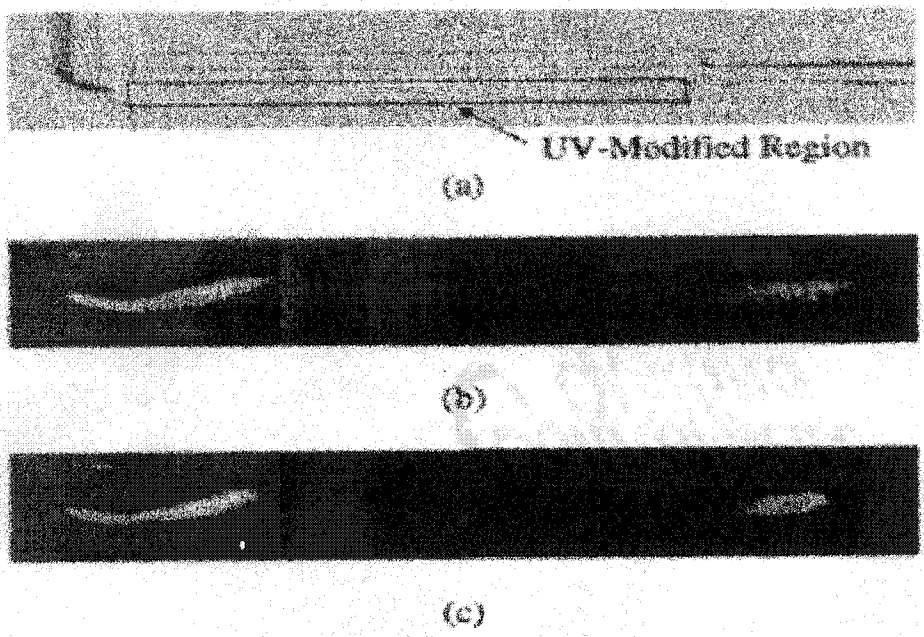

Figure 4: Images of UV-Modified Turn and Resulting Unmodified (b) and Modified(c) Channel Flow (Johnson et al., 2001).

2.0 Analytical Background

This section describes the analytical background with respect to the physics of the problem, starting with the basic equations and progressing to a combined set of equations, which must be solved simultaneously. The first section will discuss the diffusion equation, the second the electrokinetic equations, the third the Navier-Stokes equations, and fourth Poisson's equation. The last two sections discuss the combined set of equations to be solved and a solution to the one-dimensional (1-D) problem, with similar initial conditions to verify the software used in the simulations.

2.1 Diffusion Equation (Fick's Second Law)

The diffusion equation is a combination of the mass conservation equations and Fick's first law to produce Fick's second law, which is also known as the diffusion equation. The equations were derived by Adolf Fick in the mid 1800's and are similar to Fourier's law for heat conduction and Ohm's law of electrical conduction (Cussler, 1997, p. 16). The original Fick's laws are shown in Equations (1) and (2). Equation (3) is used to combine Fick's first law to produce Fick's second law.

In Equation (1), c represents concentration, t represents time, x represents a physical dimension and J represents the flux of a species through an arbitrary area. This is known as the concentration conservation equation.

$$\frac{\partial c}{\partial t} + \frac{\partial J}{\partial x} = 0 \qquad (1)$$

In Equation (2), D represents the diffusion constant of a fluid, and v represents the velocity of a species through a unit area. This is known as Fick's first law.

$$J = -D\frac{\partial c}{\partial x} + cv \qquad (2)$$

Equation (3) defines Fick's second law and it is a combination of Fick's first law and the conservation concentration equation.

$$\frac{\partial c}{\partial t} - \frac{\partial}{\partial x}(cv - D\frac{\partial c}{\partial x}) = 0 \qquad (3)$$

In Equations (2) and (3), there is a secondary component, 'cv', which is defined as the flux of concentration 'c' traveling at velocity 'v' through a plane. This additional term will be used later to combine the electrokinetic and the diffusion terms.

2.2 Electrokinetics Equations

Before the three simulation equations are derived, the physical theory of electrokinetics will be discussed briefly and the effect it has on the flow of the fluid and the concentration. The two flow components, electroosmotic and electrophoretic, will be separated and discussed individually.

2.2.1 Electroosmosis

Electroosmotic flow in a channel or tube with a charged surface is generated by the application of an electric field. A neutral fluid with positive and negative ions normally has an even charge distribution, but inside of a charged channel or tube some of the ions will tend to be distributed close to the walls of the channel to counteract the surface charge. The result of this distribution is that the bulk of the fluid far from the wall will have a mild non-neutral charge distribution. In the presence of an electric field, this distribution will generate a flow which will have drag-like effects near the surface of

the channel. The resulting charge and electric potential distribution is shown in Figure 5. The electric field from the surface of the channel is generated by solving for the Poisson equation given as Equation (4), with the electric charge distribution given by the Boltzman distribution given in Equation (5). The result of the two equations combined is Equation (6), reduced to one dimension to represent the distance from the surface of the channel (Probstein, 1989). In Equations (4), (5), and (6), ρ_e is the charge density, ε is the permitivity of the medium, F is the Faraday constant, R is the gas constant, c_0 is the initial concentration, T is the temperature, y is the dimension perpendicular to the surface, z is the ion charge, and ϕ is the electric field.

$$\nabla^2 \Phi = -\frac{\rho_e}{\varepsilon} \tag{4}$$

$$\rho_e = -2Fzc_0 \sinh\left(\frac{zF\phi}{RT}\right) \tag{5}$$

$$\frac{d^2\phi}{dy^2} = \frac{2zFc_0}{\varepsilon} \sinh\left(\frac{zF\phi}{RT}\right) \tag{6}$$

Equation (6) is then linearized to produce Equation (7). The limitation of the linearization is that the channel width is large, and error from the simplification can be quite large with a channel width of less than 10 microns. In Equation (7), λ_D is defined as the Debye-Huckel length, which is evaluated by an equation that equates the thermal forces and the electric forces, and is shown in Figure 5.

$$\frac{d^2\Phi}{dy^2} = \frac{\Phi}{\lambda_D^{\,2}} \tag{7}$$

Figure 5 also shows the distribution of the potential close to the surface as based on Equation (7), with an initial condition of Φ_w at x=0. This potential condition Φ_w is most

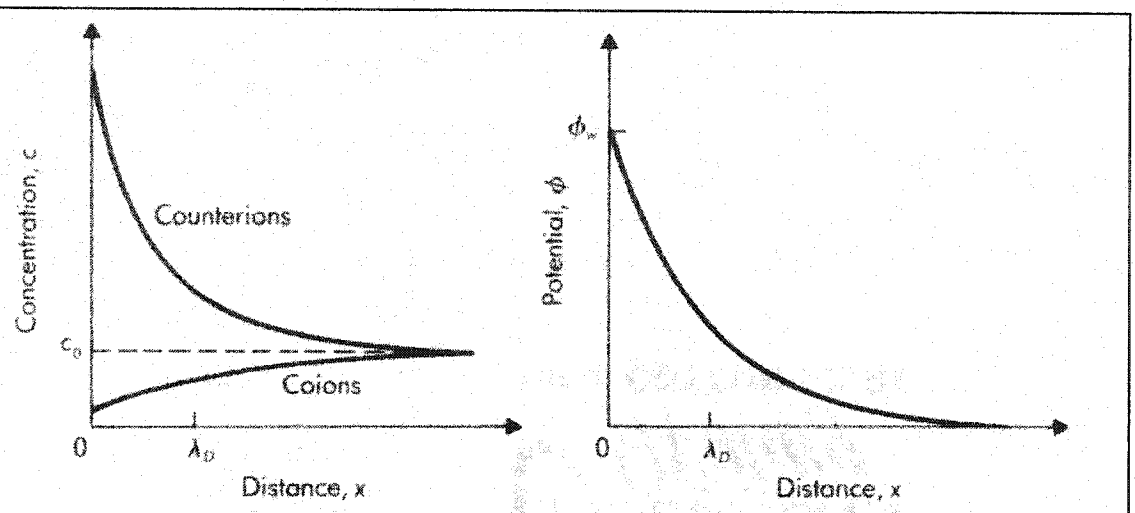

Figure 5: Relationship of Ion Balance to Electric Potential with Debye-Huckel Length (Probstein, 1989).

often referred to as the zeta potential and will be represented by ζ later. For x outside of the graph, the potential reaches nearly zero at range of 10 nm, and represents the position of thermal and electric force balance (Probstein, 1989). The edge of the channel is normally in the region in the range -10nm < x < 0, only an atom or two wide, and several models have been proposed to more accurately determine the zeta potential (Probstein, 1989).

Further from the edge of the channel are the bulk effects that the electric potential distribution has on the bulk fluid flow. First, the Navier-Stokes equation including the electric field term is rearranged so that the momentum due to the electric potential in the flow direction is shown. In the equation, ρ, $\vec{u}$ u, t, $\vec{\tau}_{ij}$, y, $\vec{g}$, ρ_E, and $\vec{E}$ represent the

density of the fluid, velocity of the fluid, time, shear stress on the fluid in tensor notation, a generic physical dimension, the vector of gravity, the charge density of the fluid, and the electric field. The subscripts i and j represent various coordinates in a cartesian coordinate system. For example, in three dimensions, i, j would designate the x, y, and z coordinates.

$$\rho \frac{D\vec{u}}{Dt} = \nabla * \frac{\partial \vec{\tau}_{ij}}{\partial y_j} + \rho \vec{g} + \rho_E \vec{E} \qquad (8)$$

Neglecting gravity and the pressure-based terms (almost no pressure gradient), Equation (8) simplifies further to a relationship based on only the viscous and the electric forces (Probstein, 1989). This relationship is shown in the balance equation for electric and viscous forces in a body of fluid.

$$\mu \nabla^2 \vec{u} = -\rho_E \vec{E} \qquad (9)$$

If Equation (9) is reduced to one dimension, and ρ_E is replaced by Poisson's equation, Equation (10) is the result. Here μ, Φ, E_x, and ε represent the dynamic viscosity of the fluid, the electric potential of the fluid, the electric field in the x direction, and the permitivitty of free space, respectively. The symbol u represents the flow perpendicular to the coordinate system, y. The logic here is the Debye-Huckel approximation dictates the charge distribution from the channel, represented by ρ_E.

$$\mu \frac{\partial^2 u}{\partial y^2} = -\rho_E E_x = \varepsilon \frac{\partial^2 \Phi}{\partial y^2} E_x \qquad (10)$$

Integrating Equation (10) twice with respect to y results in an equation that can be solved for the velocity, and Equation (11) is the result. The boundary conditions far away from the channel surface ($y = \infty$) are $\partial u / \partial y = \partial \phi / \partial y = 0$ and for the speed of the fluid at the surface (u = 0), the boundary condition is $\Phi = \zeta_{EO}$. Equation (11) is often used to determine the electroosmotic flow speed of a fluid (Probstein, 1989).

$$U = -\frac{\varepsilon \frac{\partial \Phi}{\partial y} E_x}{\mu} = -\frac{\varepsilon \zeta_{EO} E_x}{\mu} = \mu_{eo} E_x \qquad (11)$$

When the Debye-Huckel length is extremely small, the effect on the flow is a nearly flat velocity profile which is proportional to the applied electric field, the viscosity of the fluid, the electric permitivity, and the zeta potential (Probstein, 1989).

2.2.2 Electrophoresis

Electrophoresis is modeled in a similar manner than electroosmosis is, with the exception that the generated equation is without a minus sign. The differences in sign arise from differing boundary conditions when solving the Poisson equation in one dimension, and $0 < x < +\infty$. For electrophoresis, the boundary conditions are based on the radius of the particle and the electric potential, with ϕ=0, u=0 far from the surface of the particle, and $\phi=\zeta_i$, u=U at the surface of the particle (Probstein, 1989).

$$U = \frac{\varepsilon \zeta_i E_x}{\mu} = z_i \mu_{ep,i} E_x \qquad (12)$$

In the equation above, the electrophoretic mobility, $\mu_{ep,i}$ of a particle, i, is used in conjunction with the charge quantity, z_i to determine the speed of the particle. Typically,

this charge quantity is the charge of the particle that is being driven with the voltage. The zeta potential in Equation (12) reflects the potential at the surface of the particle rather than of the wall of the channel (Probstein, 1989).

2.3 Navier-Stokes Equations

The Navier-Stokes equations are shown below, and as they are a bit tedious to derive, the reader is suggested to consult a good book on the subject for more detailed information. The website Amazon.com has a multitude of books on the subject, such as *Navier-Stokes Equations: Theory and Numerical Analysis*, by Roger Teman. For proper conservation of flow, three equations are needed, the mass, momentum, and energy conservation equations. The general mass conservation equation is shown in Equation 13 (CFDRC Module Manual, 2001):

$$\frac{\partial \rho}{\partial t} + \nabla \bullet (\rho \vec{V}) = 0 \qquad (13)$$

The general momentum conservation equations are reduced to the following equations (CFDRC Module Manual, 2001):

$$\frac{\partial (\rho u)}{\partial t} + \nabla \bullet (\rho \vec{V} u) = -\frac{\partial p}{\partial x} + \nabla \bullet (\mu \nabla u) + S_{Mx} \qquad (14a)$$

$$\frac{\partial (\rho v)}{\partial t} + \nabla \bullet (\rho \vec{V} v) = -\frac{\partial p}{\partial y} + \nabla \bullet (\mu \nabla v) + S_{My} \qquad (14b)$$

In Equation (14a, b), u, v, S_{Mx}, and S_{My} represent the velocity of the fluid in the x direction, the velocity of the fluid in the y direction, the sum total of other external forces in the x direction and the sum total of the forces in the y direction. There is no internal energy creation, and the temperature and pressure are assumed constant, so the energy

equation does not need to be solved. The additional external forces are added to the above equations and these components are discussed in the combined equations section.

2.4 Poisson's Equation

The third equation is the equation for the electric potential. The electric field is solved through the Poisson equation, and is given by Equation (15):

$$\nabla^2 \Phi = -\frac{\rho_e}{\varepsilon} \tag{15}$$

Here, Φ is the electric potential, ρ_e is the charge density of the fluid (assumed constant for this case) and ε is the permittivity of the fluid. The electric field is then calculated in the appropriate direction depending on the cell in the volume being modeled.

2.5 Combined Equations

The components above are all combined to produce a system of equations that need to be solved simultaneously. A modern CFD program was available and used to study the two-dimensional (2-D) problem. The 1-D analytical solution and the 1-D computed solution are compared and verified later to judge the effectiveness of the software.

The first equation is the diffusion equation, similar to Equation (3), with some minor changes from the electrokinetic phenomenon. Electrophoresis is modeled according to the third term in Equation (16), as an additional momentum term, affecting the species in the sample only. The flow from electroosmosis is in the second term, and is linked to the Navier-Stokes equations as described before. In the equation, z_i is the charge of the ith species, ω_i is the electrophoretic mobility, D_i is the diffusion constant,

and ϕ is the electric potential of the fluid. This equation is also known as the Nerst-Plank equation (CFDRC User Manual, 2001).

$$\frac{\partial c_i}{\partial t} + \frac{\partial}{\partial x_j}(u_j c_i - z_i c_i \omega_i \frac{\partial \phi}{\partial x_j} - D_i \frac{\partial c_i}{\partial x_j}) = 0 \qquad (16)$$

In Equation (16), i is the number of species in the fluid, and j is a number from 1, 2, and 3, and represents the x, y or z coordinates from a cartesian coordinate system. For example, with one species, and two dimensions, there are two equations. Thus there is one equation each for the x, y, and z concentration flux.

The second equation is the Navier-Stokes equation, which is the primary equation used to describe the flow of the fluid (CFDRC User Manual, 2001). The last term in Equation (17) is the electroosmotic flow term, which as derived earlier, adds a bulk flow to the fluid. In Equation (17), κ^2 is equivalent to $1/\lambda_D$, with λ_D defined as the Debye-Huckel length.

$$\frac{\partial}{\partial t}\rho u_i + \frac{\partial}{\partial x_j}\rho u_j u_i = -\frac{\partial p}{\partial x_i} + \frac{\partial}{\partial x_i}\mu[\frac{\partial u_i}{\partial x_j} + \frac{\partial u_j}{\partial x_i}] + \varepsilon \kappa^2 \varsigma \frac{\partial \phi}{\partial x_i} \qquad (17)$$

Equation (17) is in tensor form and when expanded into x and y components, results in two different equations that need to be solved simultaneously.

The third equation is the Poisson equation, as Equation (15) above, with no modifications. The electric permitivitty is constant, as the fluid is nearly uniform, and the charge density is set based on the fluid properties.

2.6 Analytical Solution

The analytical solution to the one-dimensional problem, assuming negligible edge effects, is derived here for comparison to the CFD-ACE+ software results and for calibration purposes. A one-dimensional diffusion equation is shown in Equation (18) and is known as Fick's Law of Diffusion. The solution to the equation for the one-dimensional infinite case, with an initial condition equal to the Dirac-delta function at x=0, t=0, is given in Equation (19).

$$\frac{\partial c}{\partial t} = D\frac{\partial^2 c}{\partial x^2} \tag{18}$$

$$c(x,t) = \frac{1}{(\pi Dt)^{1/2}} e^{\frac{-x^2}{4Dt}} \tag{19}$$

The species moves in proportion to the electric field, and thus has a velocity component. The velocity term is added to Equation (18) to produce Equation (20) and is referred to as the advection-diffusion equation. The solution to which should be obvious and adds a velocity, or time dependent translation term to the solution, as Equation (21).

$$\frac{\partial c}{\partial t} = D\frac{\partial^2 c}{\partial x^2} + U\frac{\partial c}{\partial x} \tag{20}$$

$$c(x,t) = \frac{1}{(\pi Dt)^{1/2}} e^{\frac{-(x+Ut)^2}{Dt}} \tag{21}$$

The initial condition for the methods tested here is not the impulse function, but a square profile as illustrated in Figure 6. Fick's Law is nearly identical to a version of the heat conduction equation, so the solution to this equation may be obtained with a replacement of variables in the solution of a heat conduction equation. Based on this relation, the solution to the problem with a range of $0 > x > +\infty$ and an initial condition as given in Figure 6 is given in Equation (22). This result is used to validate the simulation software to a previously derived analytical solution, and will be discussed in the results section (Gebhart, 1993).

$$\phi = \frac{c - c_i}{c_1 - c_i} = \frac{1}{2}\left(erf\left(\frac{s-(x-vt)}{(2\sqrt{Dt}}\right) + erf\left(\frac{s+(x-vt)}{2\sqrt{Dt}}\right)\right) \qquad (22)$$

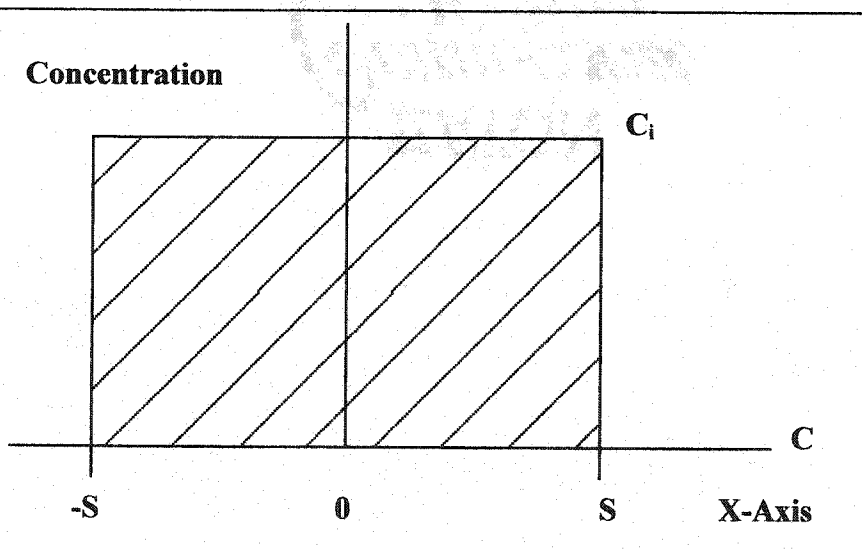

Figure 6: Initial Condition Concentration Distribution at T=0.

3.0 Numerical Background

Several methods were used in this study to generate numerical solutions. The software used is capable of studying the effects of multiple physical phenomenon at the same time. This section discusses how the software models the physics of the problem. First, the flow equations are discussed, along with some of the details of how the software reduces each term to standard finite-volume equations. Fine details of the numerical methods used to generate the solutions here are not given, and may be retrieved from the software company on request. Finally, the summation methods used for each cell in the numerical model are then discussed, with details as to how the error in a solution is calculated by each method.

The software used to model the physics of the problem is CFD-ACE+, courtesy of CFD Research Corporation. It models the electric field first, and then calculates the fluid aspects of diffusion, and the associated pressure and velocity based on Navier-Stokes equations. It uses an iterative method to determine the solution, with each physical property (electric potential, concentration) adding to the solution as a separate source term. Originally designed as computational fluid dynamics (CFD) software the computations are performed using a finite volume method.

The problem modeled here is significantly simplified in comparison to the capabilities of the software. A graphics user interface allows the user to construct the volume in three-dimensions (3-D) through the CFD-GEOM package and it is also possible to import shapes through various CAD formats. Scripting and customizable programming is possible through the Python programming language and also through

Fortran for customizable physics. Many of the common iterative schemes are already pre-programmed, and assuming the user has some knowledge of the physics of a particular program, it is possible to program almost anything with a minimal amount of effort. Most of the common physical phenomenon are pre-programmed into the software and can be activated individually or at same time through a graphical user interface. Initial conditions and boundary conditions may all be specified by the same user interface. Each individual physics phenomenon is selectable under the graphics user interface, allowing multiple physics phenomenon to be modeled simultaneously. For this thesis, the software uses the flow, electric, and chemistry modules. The chemistry module is used to include the properties of various species depending on the configuration. The electric module is used to model the electric field effects near the channel walls and to evaluate the fields in the turn. The flow module is used to conserve for the various forces on the fluid and to "tie in" all of the various physical components. Other modules included with the software are heat transfer, turbulence, user scalar, radiation, cavitation, grid deformation, stress, magnetic, electroplating, bio-chemistry, spray, free surface, plasma, and a two-fluid module. The power of being able to model multiple different physical phenomenon at the same time while having a minimal error is a very powerful feature and will likely be the trend for future modeling as it saves some time and money in experimentation costs. As computers get more powerful and the company builds a database of all the various physics that can be modeled, coupled with verification studies of the software, almost anything will be able to be modeled in the future. This also addresses the demand that companies must stay on the cutting edge of technology, and a

company may make modifications to a physical model and tested without having the expense of manufacturing a prototype. Contact may be made to the company through the following address:

CFD Research Corporation

215 Wynn Drive

Huntsville, AL 35805, USA.

Tel: (256)726-4800

Fax: (256)726-4806

Email: info@cfdrc.com

3.1 Iterative Methods

The flow equations modeled by the software are the Navier-Stokes equations, and, as explained in the previous section, the resulting equation to be solved for the thesis is given as Equation (17). In addition, the diffusion equation, Equation (16), along with Poisson's equation, Equation (15), needs to be solved for each of the finite volume cells. Figure 7 shows a diagram of a generic cell topography and is used as a reference for these equations.

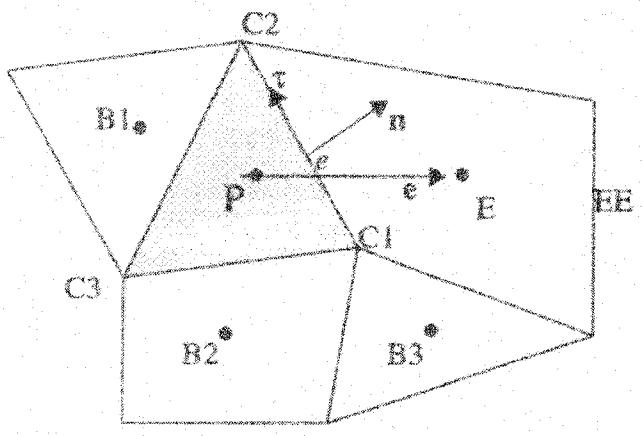

Figure 7: Typical Cell Geometry with Notations (CFDRC User Manual, 2001).

These simplified equations were discretized by CFD-ACE+ through the following series of equations, and further details can be retrieved through CFD Research Corporation (CFDRC User Manual, 2001).

For the transient terms:

$$\int_{\upsilon}\frac{\partial(\rho\phi)}{\partial t}d\upsilon = \frac{\rho\phi\upsilon - \rho^{o}\phi^{o}\upsilon^{o}}{\Delta t}$$

ϕ is the velocity of the fluid, as u, v, or w; υ = control volume of cell; ρ=density of the fluid; o = older time.

For the convective terms:

$$\int_{\upsilon}\nabla\bullet(\rho\vec{V}\phi)d\upsilon = \oint_{A}\rho\phi\vec{V}\bullet\vec{n}\,dA = \sum_{e}(\rho_{e}\phi_{e}V^{n}{}_{e})A_{e} = \sum_{e}C_{e}\phi_{e}$$

Whereas C_e is the mass flux across the surface 'e' of the cell volume, A_e is the surface area of the cell in the direction of the normal vector $\vec{n}$, and V_e^n is the velocity component in the direction of the normal vector.

For the diffusion terms, discretization of the integral is as follows:

$$\int_{\upsilon}\nabla\bullet(\Gamma\nabla\phi)d\upsilon = \int_{A}\Gamma\nabla\phi\bullet\vec{n}\,dA = \sum_{e}\Gamma_{e}(\frac{\partial\phi}{\partial n})_{e}A_{e}$$

$$\frac{\partial\phi}{\partial n} = \frac{1}{\vec{n}\bullet\vec{e}}(\frac{\partial\phi}{\partial e} - \vec{e}\bullet\vec{\tau}\frac{\partial\phi}{\partial\tau})$$

$$\int_{\upsilon}\nabla\bullet(\Gamma\nabla\phi)d\upsilon = \sum_{e}\frac{\Gamma_{e}}{\vec{n}\bullet\vec{e}}(\frac{\partial\phi}{\partial e}) - \sum_{e}\frac{\vec{\tau}\bullet\vec{e}\,\Gamma_{e}}{\vec{n}\bullet\vec{e}}(\frac{\partial\phi}{\partial\tau})_{e}A_{e}$$

$$(\frac{\partial \phi}{\partial e})_e = \frac{\phi_e - \phi_P}{\delta_{P,E}}$$

$$(\frac{\partial \phi}{\partial \tau})_e = \frac{\phi_{C2} - \phi_{C1}}{\delta_{C2,C1}}$$

In which Γ_e is the diffusion coefficient of cell 'e', $\vec{n}$ is the normal vector bordering the edge of the 'P' and the 'E' cells, $\vec{e}$ is the vector from the center of cell 'P' and the center of cell 'E', P is cell P, E is cell E, δ is the distance between two pts (ie, center of P, center of E, node C1, node C2) and τ is the vector defined by C1, C2.

Three simulations composing two sources are used here to validate the software solutions to the analytical solution from general equations. These simulations and their discussion are given in the results and discussion of the results section. In addition, turn simulations are used to compare the CFD-ACE+ results to available experimental data in the same sections.

Multiple finite-volume differencing schemes were used to produce the outputs depending on the initial and boundary conditions. The differencing schemes used were the most common methods used in finite volume analysis, including some schemes which were proprietary. Such schemes include first-order upward, central, second order upward, second order upwind with limiter, a smart scheme of proprietary nature, and a third order scheme. The goal was to find the particular scheme that produced a convergent solution while not requiring excessive time to achieve the solution (CFDRC User Manual, 2001).

Four different outputs were calculated when running the numerical simulations, which were the pressure, velocity, electric potential, and concentration. For each of the parameters solved, a particular spacial and temporal differencing method was selected for the position and temporal derivatives of the outputs, respectively. This set of difference equations was then solved using an iterative linear method, rather than a direct solver. While there are no perfect solutions to an iterative method, there is a residual output for each parameter solved. These residual outputs represent the accumulated sum of the errors from each cell from the previous iteration. This residual was the most important in determining the "quality" of the solution, and through experimentation, a residual of 10^{-6}, was deemed the "point of diminishing returns," where a smaller residual did not seem to improve the solution from the simulation.

3.2 Assumptions and Limitations

For the simulation software, mass balance for concentration is not taken into account for multiple species, and the results from the CFD-ACE+ software are reliable only for conditions where the species is a small fraction of the whole fluid and when the properties of the species are not too far distant from the bulk fluid. Heat effects from electric current are negligible, and the temperature is constant.

4.0 Conditions and Range of Variables

The initial conditions, parameters, and comparison criteria used in this thesis are discussed in this chapter. First, the initial conditions of each method are discussed, including the conditions of the current literature from the static turn changes, to the elecroosmotic flow case, and the voltage controlled method. The conditions from the current literature, including experimental results, are also listed for comparison. Following this are the comparison criteria for the techniques for comparison that are discussed later.

4.1 Turn Conditions

The initial conditions, boundary conditions, and results for the three methods here were set in the range of the studies from the current literature. Comparison criteria were from the current literature and the results from the literature used to compare the three techniques simulated with the CFD-ACE+ software. The initial conditions of the problem are now discussed, from the static turn cases to the electroosmotic flow cases, based on results from available literature. Conditions from the literature, including experimental results, are also listed for comparison.

4.1.1 Turn Conditions--Numerical

Geometry values were chosen close to experimental results from a paper recently published (Culbertson et al., 1998). Figure 8 shows the geometry of the CFD-ACE+ simulations. The length to the turn is long for these simulations to ensure that a typical species that has already encountered some diffusion enters the turn. It is kept fixed to reduce the effect that this added length has on the solution. The parameters studied most

Table 1: Table of Geometry Conditions for Three Different Width Ratio Cases Studied (Units in μm).

Length of Turn	3000	3000	3000
Width of Channel (a)	177	177	177
Length to Sample	180	180	180
Length of Sample	180	180	180
Radius of Turn (r)	2	73	1000
δ (For further Analysis)	1.96	1.10	0.16
Total Cells	5720	9320	13260

extensively in the past were the effect of width-radius ratio, defined by δ in Equation (23), and was varied to get three cases at the extremes of the tests done in published literature for comparison and verification (Griffiths & Nilson, 2000). In each simulation, the CFD-ACE+ cell geometry was changed so that the solution was valid for each of the cases. There appears to be limited data in the three cases, but the interest here was to compare the extremes and to complement what was offered by the literature, not to provide a full range of data for all δ cases. Table 1 presents the geometry conditions for the turn problem. The symbol 'δ' represents a ratio as generated by Griffiths and Nilson, given in Equation (23) (2000).

$$\delta = \frac{\bar{r}}{a} = \frac{r + a/2}{a} \qquad (23)$$

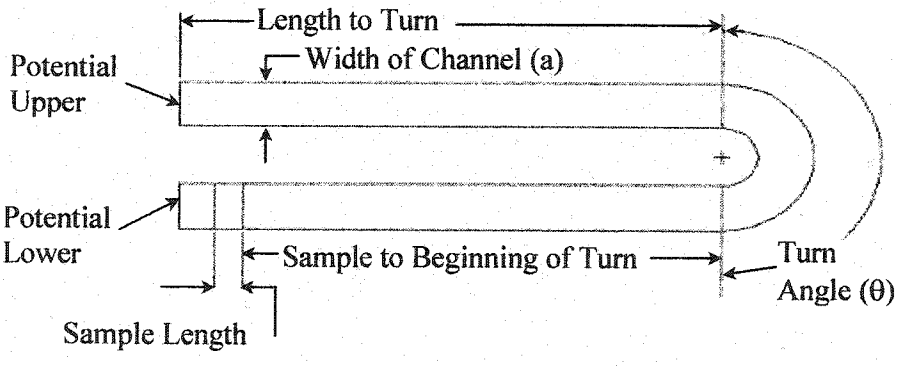

Figure 8: Diagram of Geometry for Finite-Volume Study.

In the equation, r is the radius of the turn and a is the width of the channel. Other variables that define the geometry involve the distance to the beginning of the turn, the width of the sample, and the distance of the sample to the beginning of the turn, as shown in Figure 8.

For the simulations, the turn was separated into five sections, with the upper edge of the turn composed of one section, the bottom separated into 3, and the inverted 'c'

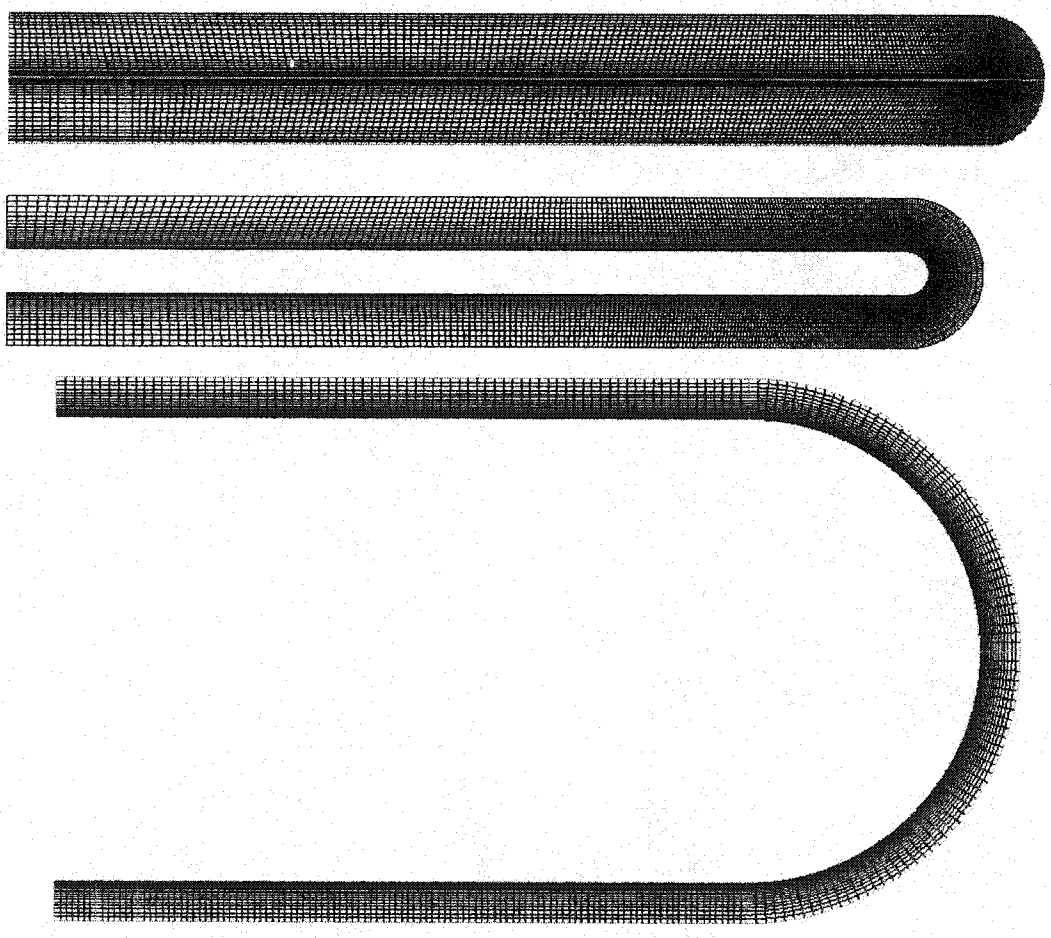

Figure 9: Cell Graphs for Small, Medium, and Large Radius as Modeled in CFD-ACE+ Software. Graphs Generated with CFD-GEOM Software.

shape separated into 2 pieces. The generated cell geometry was denser near the inner edge of the turn to ensure better results. The total number of cells for the three simulated geometries is given in Table 1 with the cell geometry shown in Figure 9 and a magnified view near each of the turns is shown in Figure 10.

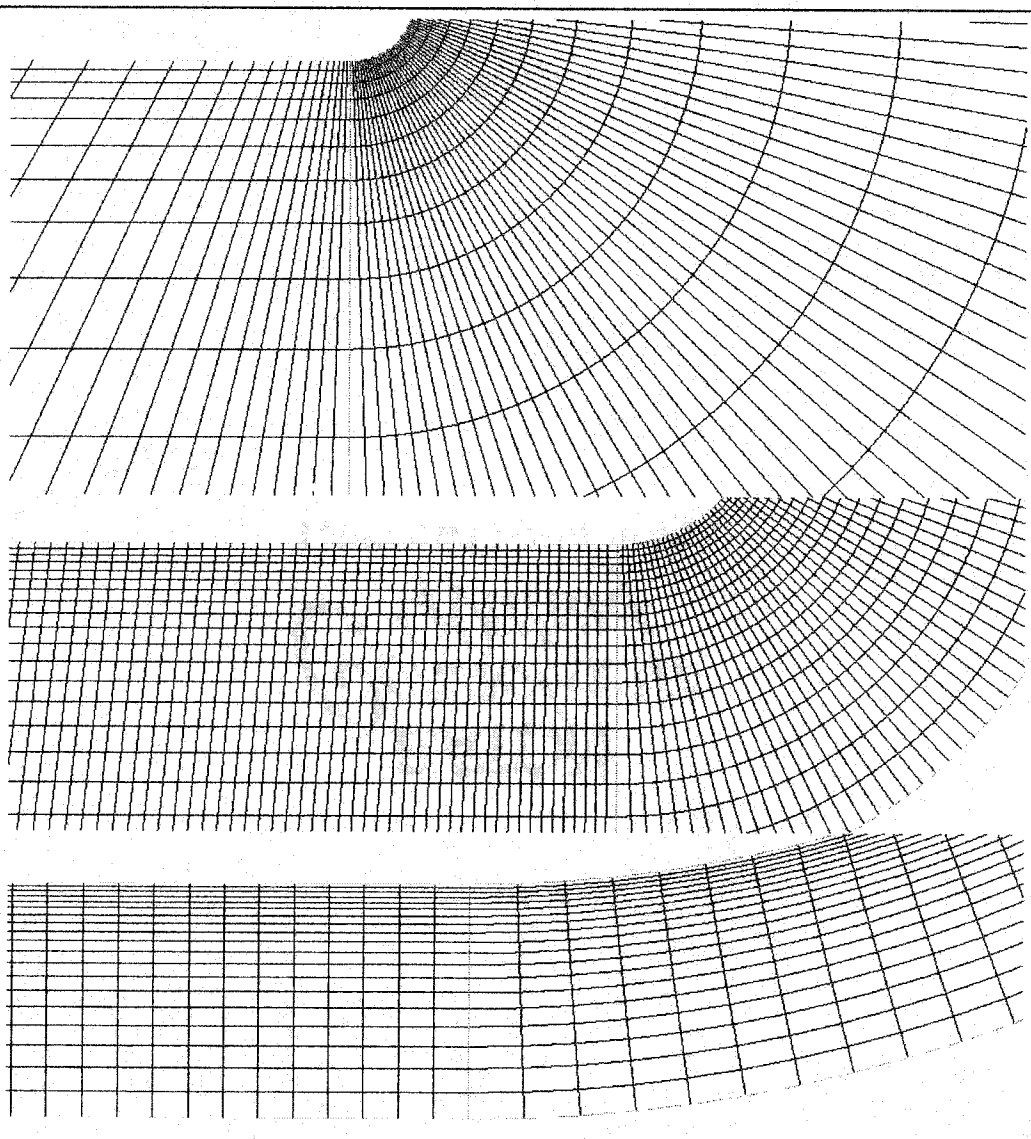

Figure 10: Close Up View of Corner for Small, Medium, and Large Radius Turns. Graphs Generated with CFD-VIEW Software.

Table 2: Physical Parameters Used in Simulations.

Material	As Water	As Sample
Pressure (Relative--as Atm)	1	1
Initial Velocity (m/s)	0	0
Density (kg/m^3)	997	997
Temperature (K)	300	300
Dynamic Viscosity(km/m s)	8.55E-4	8.55E-4
Relative Permitivitty	1	1
Electrical Condictivity (1/Ohm m)	0.0001	0.0001
Charge (as electron)	0	1
Electrophoretic Mobility	0	As Data Point--Of Order 1E-7/8
Electroosmotic Mobility	0	0--Assumed EOM similar to EPM
Diffusivity	0	As Data Point--Of Order 1E-9/10
Domain Voltage Differential(V)	30	30

Before a simulation was started, a cell quality check was performed on the geometry. This quality check as performed by the software determines the smallest angle inside of the cell. Cells of too small of an inside angle (see Figure 11) may add excessive error to the solution. Figure 11 shows an illustration of the 4-sided cell used in the

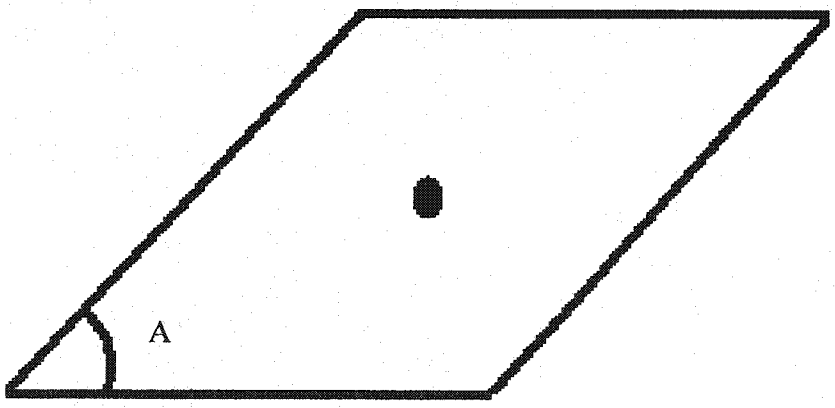

Figure 11: Diagram of Cell Minimum Internal Angle.

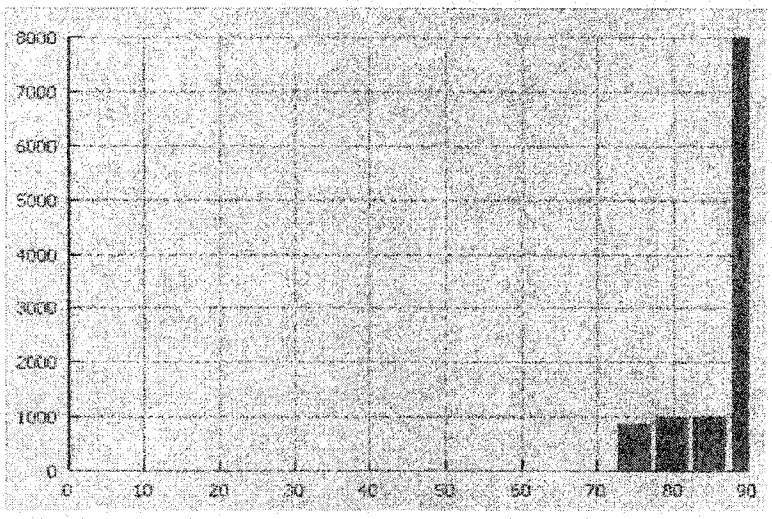

Figure 12: Minimum Cell Internal Angle (X-Axis) vs Total Cell Number with δ=0.16. Graphs Generated with CFD-GEOM Software.

studies here. In the figure, the angle 'A' represents the smallest internal angle of the cell. A branch manager of CFD Research Corporation, Dr. Metin Ozen, recommended that cells not have an inner angle less than 45 degrees. Figures 12, 13, and 14 show the minimum internal angle versus the number of cells in a histogram format. The simulation with the small radius had the most number of cells with small internal angle, which was as expected due to the high density of cells in the turn area.

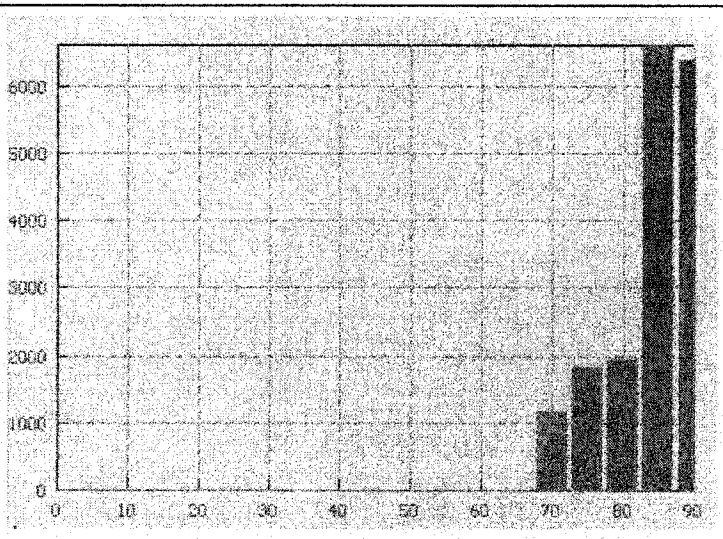

Figure 13: Minimum Cell Internal Angle (X-Axis) vs Total Cell Number with δ=1.10. Graph Generated with CFD-GEOM Software.

The physical properties for the fluid in the CFD-ACE+ turn simulations are shown previously in Table 2. The physical conditions of the turn simulations with CFD-ACE+

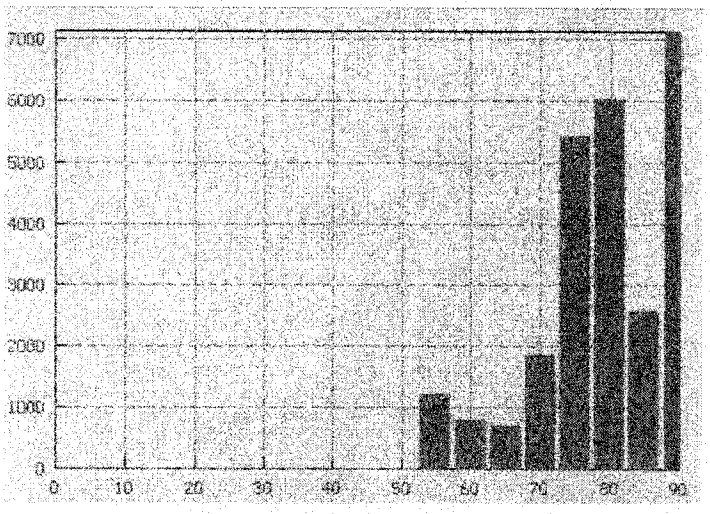

Figure 14: Minimum Cell Internal Angle (X-Axis) vs Total Cell Number with δ=1.96. Graph Generated with CFD-GEOM Software.

software were set so the test sample concentration was 100 percent in the sample section as shown in the geometry of Figure 8 and was 100 percent water in the other section. The only major differences between the two fluids, as noted in Table 2, were from the diffusivity and EP mobility. In the case of the turn simulations, EO flow was assumed similar to EP flow to reduce the number of computations. This assumption is valid under the following criteria:

The flow is laminar.

There are no other forces on the fluid other than electrokinetic phenomenon.

The Debye-Huckel length is small in comparison to the channel width.

Equations (11) and (12) are used to dictate the EO and EP flows.

The condition for laminar flow is given by a low Reynolds number, which is around 0.1 given the data in Table 2 and an EO velocity of 1 cm/s using Equation (24) (Probstein, 1989, p. 48).

$$\mathrm{Re} = \frac{Ua}{\nu} \qquad (24)$$

Table 3: Simulated Electroosmotic Flow Initial Conditions.

EO Mobility (m^2/Vs)	1E-8 to 2E-10
EP Mobility (m^2/Vs)	1.00E-09
Diffusivity (m^2/s)	3.44E-11
Peclet Number(highest)	790
Ratio EO Upper/Lower	0-18%, by 2 %
Zeta Potential(V)	As Per Equation 8
Debye-Huckel Length(m)	1E-8
Domain Voltage Differential(V)	30

4.1.2 Turn Conditions- Literature

Two papers, one involving experimental data, and one involving simulated data, are used to compare to the results of the finite element simulation done with the CFD-ACE+ software. The first paper, as described previously, is the paper written by Culbertson et.al, from the Oak Ridge National Laboratory in 1998, and includes experimental data. The second paper includes simulated data from a Monte Carlo method as done by Griffiths and Nilson at Sandia National Laboratories. Here the conditions for each of the simulations as performed by these authors are presented (Griffiths & Nilson, 2000).

In the experimental study, the geometry was an 'S' shape, as shown in Figure 15, with the dimensions and geometry shown. The letter 'r' represents a specific radius, in which the experiments involved radii of 125, 250, and 500 μm. The widths of the channels for the three cases were 47 for the 500 μm, and 60 for the 125 μm radius channels. The width of the 250 μm radius channel was not given (Culbertson et al., 1998).

Standard laboratory apparatus were used in acquiring the results from the Culbertson paper, and a detailed description of the apparatus is not given here. For the

specific details of the apparatus, it is suggested the reader check the paper for more of the details. A large variety of buffers and reagents were used in the acquisition of the data as well, and it is again suggested here that the reader investigates the paper for further information. For the experiments, however, the electric field strength here was 5000 V/m with analyte mobility constants of 1E-8 to 4.24E-8 m^2/V s. In one case, the diffusion constant for a particular analyte was 2.8E-10 m^2/s (Culbertson et al., 1998).

For the simulations done by Griffiths and Nilson, a complex method was used to solve the problem, similar to a finite element method, with a few variations. The authors first normalized most of the variables in the problem, then, using a complex scheme, transformed the turn into a rectangular, rather than a 'U" shape domain. The electric potential and a stream function similar to the flow velocity served as the independent values in the transformed method. The boundary conditions of the u-shaped turn were then mapped into the transformed domain using Cauchy-Reimann compatability relations. The transformation, as described by the authors, converts the geometry of the turn into the new domain even when the internal radius of the turn is close to zero. Further details of this method are available through the authors of the paper. A Monte Carlo method was used to simulate the species transport,

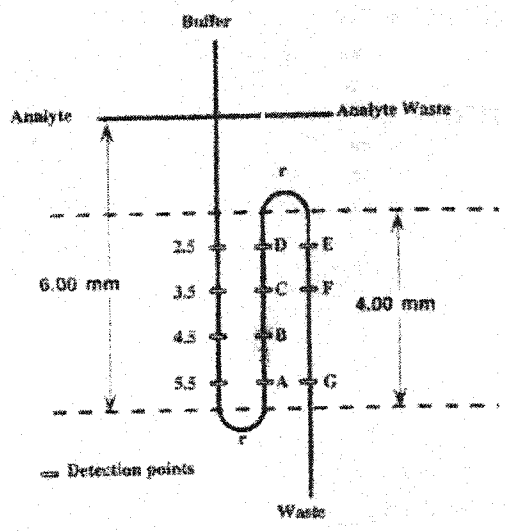

Figure 15: Diagram of Culbertson Experiments (Culbertson et al., 1998).

and the method does not generate artificial numerical diffusion, as explained in the paper. One thousand tracer particles were used to simulate the species as it traverses the transformed domain. The problem was normalized with the width squared (a^2) and the comparison criteria were variance and dispersion, which will be explained in more detail later. Material conditions of the fluid and the channel were not given in the paper. The paper was extensively based on the Peclet number, with a large range (1-1000) of Peclet numbers evaluated. The channels were assumed rectangular (the geometry was two-dimensional), and three different angle turns were used in the simulations, at 180, 90, and 45 degrees in the method, indicated as "θ" in Figure 8 (Griffiths & Nilson, 2000).

4.1.3 Electroosmotic Flow Change--Numerical Studies

Geometry conditions were chosen for simplicity and so that multiple simulations could be done to generate adequate data to compare with the experimental results. The channel was straight, with a length of 6000 μm. The sample was started at a position of 300 μm from the left edge of the channel and the sample was 100 μm long. The cells were smaller toward the top and bottom edges of the channel so that the cell density was higher near the walls. The total cells for the entire channel was 5400. Material properties were similar to that of Table 2, with exception to the EO and EP mobilities, and the diffusivity of the species. The EO and EP mobilities were chosen with similar Peclet numbers in the straight channel and based on the paper done by the group at NIST, and are given in Table 3. The Peclet number is a dimensionless number similar to the Reynolds number, and is the ratio of the convective to the diffusive forces on a fluid. The

Peclet number is important in understanding what happens in a diffusive-convective process such as this one, and has been noted in the current literature. For this problem, only a narrow range of initial conditions was tested, as the geometry in the experimental study was not rectangular, and was chosen to supplement the percentage change in values of the channel.

4.1.4 Electroosmotic Flow Change--Literature

The study as described previously by the group at NIST experimented with changing the zeta potential on one side of a channel wall after a 90-degree turn and a straight channel.

For the study, the straight channel tests used fields of between 5000 V/m and 75000 V/m with an average electroosmotic mobility of 6.5E-8 m^2/Vs, a diffusivity of 4.6E-10 m^2/s and electrophoretic mobility of 3.4E-8 m^2/Vs. The channel cross-sections perpendicular to the flow were trapezoidal, and had a channel width of 73 μm at the top, 25 μm at the bottom, with a 31 μm depth. This corresponded to a Peclet number with a range from 53 to 791.

For the 90-degree turn studies, the fields used in the study were 45400 V/m and 47600 V/m for the non modified and modified turn studies, respectively. The dimensions of the channel were 57.5 μm at the top, 26.2 μm wide at the bottom, and 26.0 μm deep prior to the turn and are 52.0 μm wide at the top, 29.0 μm wide at the bottom, and 26.0 μm deep after the turn. The electrophoretic and electroosmotic mobilities were as given in the straight channel case. The corresponding Peclet number was 268 for these cases.

4.1.5 Electric Field Change in Turn

For electric field control, there are a variety of techniques that could be used to actively and passively control the path of the fluid. Recent studies include switching the electric potential on and off in the three various inlets/outlets of a 'T' junction over time in order to switch the flow from one outlet to another. These methods met with some success in diverting the flow given a fixed output and two different output positions. In this case however understanding the impact on dispersion and variance after the turn, rather than trying to control which direction the movement occurs, were the objectives.

The geometry and material data for the CFD-ACE+ simulations with the electric field change is given as the standard turn conditions as discussed previously. The only

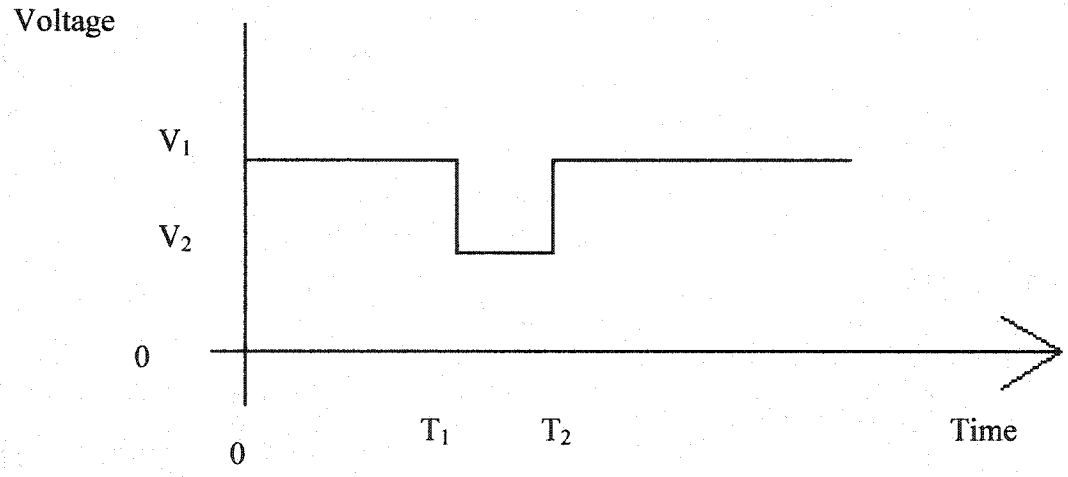

Figure 16: Diagram of Step Change inVoltage in Turn.

change was the electric field, which was stepped down near the turn to try to reduce the amount of dispersion. This change was based on simulated and literature results, as for

large Peclet numbers, there seems to be an increase in the variance for those high values. Figure 16 shows a diagram of the step change in potential for this study. Five Peclet numbers were chosen for the 3 simulations, each point corresponding to a place where a step change in potential would have the most effect. The Peclet number was then converted to a time-dependant voltage equivalent which will be explained in more detail later. For each of the simulations, a Peclet number of 1000 was chosen before the sample was anticipated to enter the turn given the electric field, electrophoretic mobility, and distance from the starting species position and the turn. The voltage was then switched back to generate a Peclet number of 1000 when the sample was anticipated to have emerged from the turn using the average radius to determine the time in the turn. The reasoning for this was to see if a reduction in the electric field in the turn reflecting a strong Peclet number reduced the variance after the turn.

Table 4: Time and Voltage Table For Step Change in Potential In Turn.

δ	ΔV To/After Turn(V)	ΔV inTurn(V)	Time to Turn(s)	Time in Turn(s)
1.96	568	568	2.07	0.78
		426	2.07	1.04
		284	2.07	1.56
		142	2.07	3.13
		56.8	2.07	7.82
0.1	851	12	2.07	25.2
		39	2.07	7.76
		66	2.07	4.59
		93	2.07	3.26
		120	2.07	2.52
1.1	589	589	2.07	0.98
		442	2.07	1.31
		294	2.07	1.97
		147	2.07	3.94
		58.9	2.07	9.85

The voltage step changes are given in Table 4. For the larger radius case,

five different Peclet numbers were chosen to highlight the dip area as described by Griffiths and Nilson and confirmed by the CFD-ACE+ simulations. The voltage change was then calculated from an electric field average across the channel.

4.2 Comparison Criteria

The comparison criteria are separated into two sections, the variables section and the equations section. The terms dispersion and variance are used as the main comparison criteria for the results of the experiments and simulations and are ultimately plotted and compared with equations developed from current literature. Another term of importance is the Peclet number, as it has been shown to be very important in the cases of the turn and the straight channel cases. These criteria are used in two equations developed from an analytical analysis and curve fitting as noted in the literature and later in the chapter.

In recent literature, the variance has been used to compare the results obtained from various methods. In one case it was calculated from an assumed square concentration profile in the electroosmotic flow experiments, and in the others by summing the concentration across the channel. Assuming a square concentration profile assumes that the distribution of the concentration in the streamwise direction after the turn is constant, but assuming a constant profile is not what occurs after the turn and has been noted in simulations and experiments previously. In cases where the radius is small it is more difficult to define and variance should be "integrated" or "summed" across the channel. This difficulty has been noted in the literature.

Dispersion is used to describe the difference between the position of the mean concentration at the near edge and the far edge of the channel. Evaluation of these criteria will be useful in determining whether the distortion after the turn is due to dispersion from the turn or more from diffusion of the species, indicated by variance.

4.2.1 Independent and Dependent Variables

The independent and dependant variables which are used to characterize the three techniques are now discussed, with their involvement in equations in the equations section. Sample calculations for each of these variables and equations are given in the sample calculation section and plotted in the results section.

4.2.1.1 Peclet Number

The relationship between the Peclet number to other constants of this problem is shown in Equation (25) (Probstein, 1989). The effects of the flow near the edge of the channel can be neglected here, as the electroosmotic flow is nearly constant across the channel with a small Debye-Huckel length. The velocity along the channel can then be described simply as the sum of the electroosmotic and electrophoretic mobilites, multiplied by the electric field. For all cases the Peclet number is calculated with the equation below, $\vec{E}$ is the electric field and a is the channel width.

$$Pe = \frac{U(c_0 - c_{T=t})/a}{D(c_0 - c_{T=t})/a^2} = \frac{Ua}{D} = \frac{\vec{E}(\mu_{eo}(y) + \mu_{ep})a}{D} = \frac{mass\ transport\ by\ convection}{mass\ transport\ by\ diffusion} \quad (25)$$

Equation (25) is valid so long as the majority of the fluid flow comes from the electrophoretic and electroosmotic effects on the fluid. The term $\mu_{eo}(y)$ describes

electroosmotic mobility as a function of the position along the cross section of the channel and will be discussed later.

4.2.1.2 Dispersion

Sample dispersion occurs when the sample traverses a turn, or other geometrical-based object, which distorts the sample from a symmetrical 1-D plane to an asymmetrical 2-D or 3-D shape. Typically, dispersion is a result of two different peaks traveling at two different velocities along a plane or from path length differences from the typical planar movement of a sample. Depending on the asymmetrical shape, distinguishing two samples with two speeds may be difficult to ascertain. If, in changing shape from the symmetrical to the asymmetrical case and one sample overlaps with another, a detector may only detect one shape from two or more overlapping peaks. If the detector can only detect one peak from one sample, there is no way to distinguish between the different species in the sample. Distinguishing one species from another is even more important in ph-gradient based studies, as the sample is not split into individual species, but graduated between the ph of the buffer solution before the sample injection and the ph of the buffer solution after the sample injection. The sample length is what is important here, and should be considerably larger than the length of the turn.

Dispersion will be calculated here as the distance between the means of cross-sections measured at the upper and lower ends of the channel after the turn. The mean position of a species may be calculated using Equation (26) and is the standard statistical mean from a series of data. Thus, dispersion may be calculated by Equation (27).

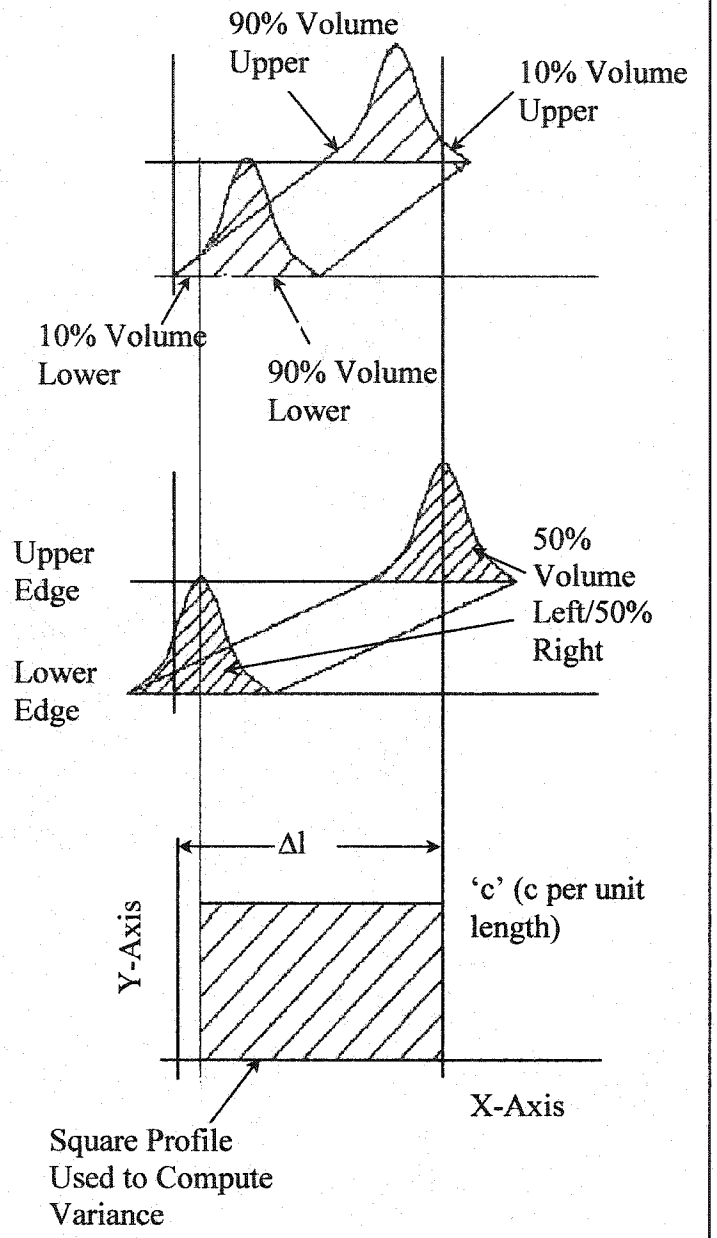

Figure 17: Diagram of Variance Calculated from a Square Profile from Two Different Authors.

In which dispersion may be calculated as follows:

4.2.1.3 Variance

Calculation of variance for this study is done with a variety of methods, as calculations through the literature have been through different methods. The first method is the standard statistical method for calculating variance, and the second is calculating variance based on an assumed rectangular concentration profile. The rectangular concentration profile is shown in Figure 17, where the concentration density from the upper edge to the lower edge as seen in a streamwise manner, is a constant, 'c'. Each of the methods are discussed and compared in the discussion of results section to see the differences. The statistical

method, which also describes the solution to the diffusion equation, is calculated through Equation (28) and samples concentrations from varying cross sections taken across the channel.

$$\bar{x} = < x > = \frac{\int xc(x)dx}{\int c(x)dx} = \frac{\sum x * C * \Delta x}{\sum C * \Delta x} \tag{26}$$

$$Dispersion = < x >_{upper\ side\ of\ channel} - < x >_{lower\ side\ of\ channel} \tag{27}$$

$$\sigma^2 = < x^2 > = \frac{\int (x - < x >)^2 c(x)dx}{\int c(x)dx} = \frac{\sum (x - < x >)^2 C * \Delta x}{\sum C * \Delta x} \tag{28}$$

The second method calculates variance from an assumed rectangular concentration distribution. Figure 17 shows this rectangular distribution. The solution to the variance of a square like profile is calculated from Equation (28), and using an arbitrary constant concentration density of 'c' corresponding to a rectangular concentration profile, the resulting variance is $\Delta l^2/12$ (Griffiths & Nilson, 2000). This solution is referred to as the rectangular variance for this thesis, with a sample calculation in the sample calculation section. The Δl term in the rectangular variance is calculated in two ways, the first being from the mean of the concentrations of cross-sections and upper and lower ends of the channel. The second method, as introduced by the NIST group, is calculated in a different manner, where the positions of the left edge and right edge are shown in the top section of Figure 17. The left edge was defined as the point at which 10% of the integrated area was to the left of the cross-section at the bottom of the channel and the right edge was calculated as where 10% of the curve was to the right of the cross-

section at the top of the channel (Johnson et al., 2001). There are also number of normalization factors for the variance established by various authors, and these are described in the equations section below.

4.3 Characterization Equations

The section here describes the equations developed by various authors. The simulations done with the CFD-ACE+ software was used to get additional comparative data to compare to these equations, and generate additional data outside of the limitations of those equations.

4.3.1 Turn Characterization

The authors Griffths and Nilson (2000) established an equation which relates the variance to the various other parameters of the problem, and is given in Equation (29). This equation was derived through an intimate knowledge of the coupled equations of the problem and is a combination of the high and low Peclet number solutions to this problem. In the equation, a is the width of the channel, δ is the width to-radius ratio as described previously, θ is the turn angle in radians, and Pe is the Peclet number. Equation (29) is the equation used to determine the variance, σ^2 of the problem with streamwise distribution, whereas Equation (30) is for the case without streamwise distribution. The minimum of Equation (29) is given in Equation (31).

$$\left(\frac{\sigma}{a}\right)^2 = \frac{\theta^2 \delta Pe}{15\theta + 3\delta Pe} + \frac{2\theta}{\delta Pe} \tag{29}$$

$$\left(\frac{\sigma}{a}\right)^2 = \frac{\theta^2 \delta Pe}{15\theta + 3\delta Pe} \tag{30}$$

$$\delta Pe = \frac{30\theta}{\sqrt{30\theta}} - 6 \tag{31}$$

Culbertson et al. (1998) also developed and studied an equation, Equation (32), which is slightly less analytical than Equation (29), with some curve fitting involved, and is more suited toward channels with non-flat walls as it includes an adjustment factor, 'X'. The variable a is the width, θ is the turn angle, the quantity t_d/t_t is the dispersion to travel time ratio as given in Equation (33), and X is the adjustment factor which may change depending on channel cross-section. The term 't_d/t_t' is described as the time ratio, and is a ratio of the time to traverse the turn (t_t) to the time to disperse across the channel (t_d). For the ratio, v_c is the velocity of the sample in the center of the channel, r_c is the radius at the center of the channel, and D is the diffusion constant. Equation (33) is similar to the Peclet number as noted by Griffiths and Nilson (2000).

$$\left(\frac{\sigma}{a}\right)^2 = \frac{2\theta(1 - e^{\left(-\frac{t_d}{t_t}\right)})^2}{X} \tag{32}$$

$$\frac{t_d}{t_t} = \frac{a^2 v_c r_c}{2D\theta(r_c + a/2)^2} \tag{33}$$

In addition to the calculations using Equations (29) and (32), the time-based variance was removed from the total variance. This is then be used to generate the scaled variance. Culbertson et al. (1998), removed the time-based variance (variance due to diffusion) from the problem by subtracting the term '2Dt' from the variance, σ^2 before normalizing with the width 'a^2' (Culbertson et al., 1998). The term '2Dt' comes from calculating the variance of Equation (19) in the one dimensional form, and is equal to

'2nDt' for multi-dimensional problems where n is the number from spacial dimensions (Tyrrell & Harris, 1984).

4.3.2 Channel Material Change

Current literature with experimental data shows that a zeta potential change to one side of the turn causes a reduction in the variance after the turn. The reduction comes from one side of the sample moving faster than the other which shortens the variance after the turn. After experimentation with different zeta potentials at opposite sides of the straight channel in the simulations tested here, it was observed that the major differences occurred only when the average Peclet number was quite low across the entire channel. When the Peclet number was high across the channel, around 400+, the sample travelled in a trapezoidal fashion down the channel, as in Figure 18. This led to the development of a speed ratio, which will be denoted the F-ratio, as described below in Equation (34).

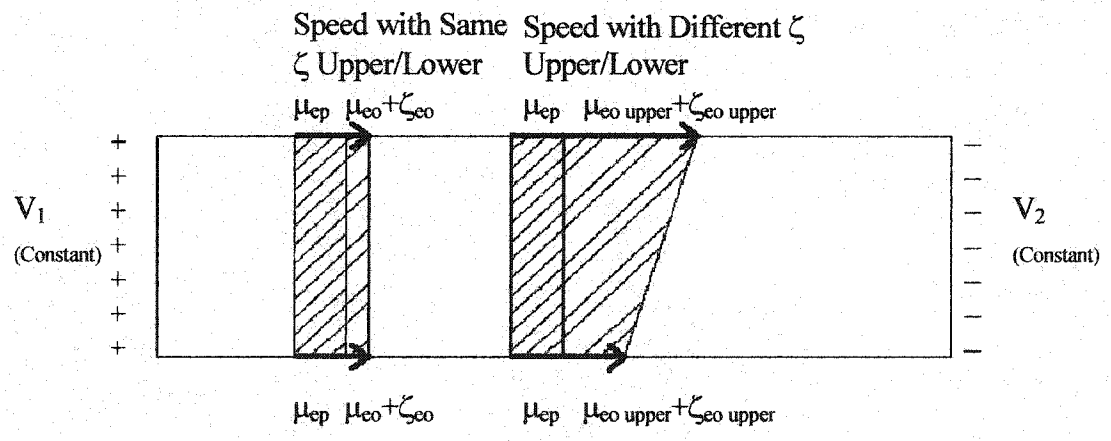

Figure 18: Profile of Flow in Channel, with Same and Differing Zeta Potential on Opposite Ends of Channel.

This ratio was developed to better understand what happens with differing zeta potentials and to reduce the amount of data.

$$F-ratio=\frac{V_{upper}}{V_{lower}}=\frac{\vec{E}(\mu_{ep}+\mu_{eoupper})}{\vec{E}(\mu_{ep}+\mu_{eolower})} \tag{34}$$

5.0 Results

The results of the experimental values and Monte Carlo simulations as described from current literature, with simulated results from the CFD-ACE+ software, are presented next.

5.1 Validation--CFD-ACE+

Validation of the CFD-ACE+ package was accomplished through three methods, with all cases being simulated in a long, narrow geometry. The first and second

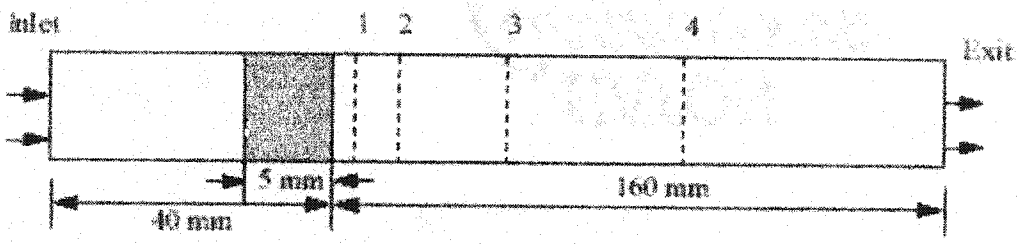

Figure 19: Initial Conditions and Geometry of Validation Study.

comparisons were done by researchers at CFD Research Corporation, using a published analytical solution (Krishnamoorthy, 2002). The third comparison was done using the software, with a slightly different measurement scheme than the first two methods.

In the first two simulations, measurements were taken at a single point over time, so the resulting charts are different from the third case. In both of these cases, the geometry was 1 mm wide and 200 mm long, with a uniform cell width of 0.5 mm thick. The integration time was set to 1 second, corresponding to a Courant, Friedrichs, and Lewy (CFL) number of 1.4E-03, considerably smaller than the numerical stability condition of 1 (Anderson et al., 1984). The scheme used was a Crank-Nicholson time

stepping scheme with a factor of 0.5 and a second order upwind scheme with a blending factor of 0 for time and spatial discretizations, respectively. The electrophoretic mobility was 2E-8 and the order of diffusion constants was 7E-10. The results of the simulations and the analytical comparison are shown in Figure 20 and 21 (Krishnamoorthy, 2002).

The third simulation was done along with the electroosmotic flow change studies for this thesis. The dimensions of the second straight channel were 6 mm long by .5 mm

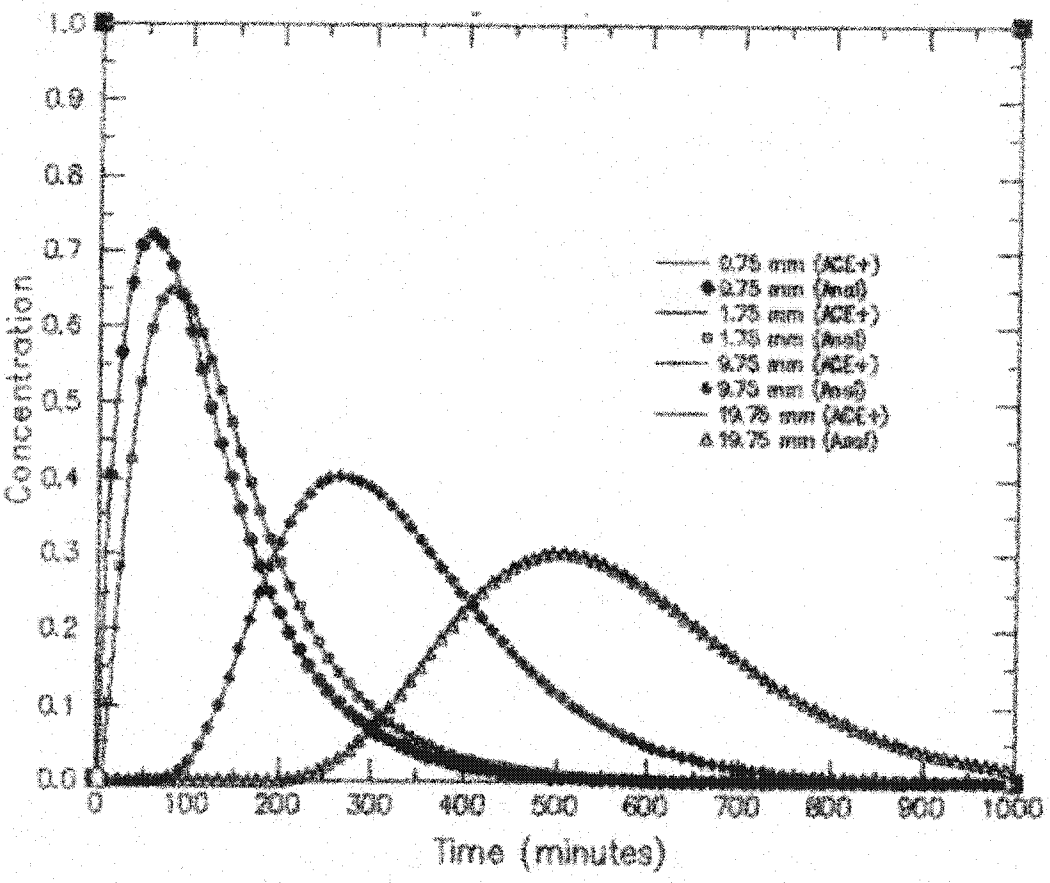

Figure 20: Concentration vs Time--Validation Studies (Krishnamoorthy, 2002).

wide, with a cell spacing of 22 μm in the length direction. There were 19 cells across the channel of varying size with the largest cells in the middle to model the electroosmotic

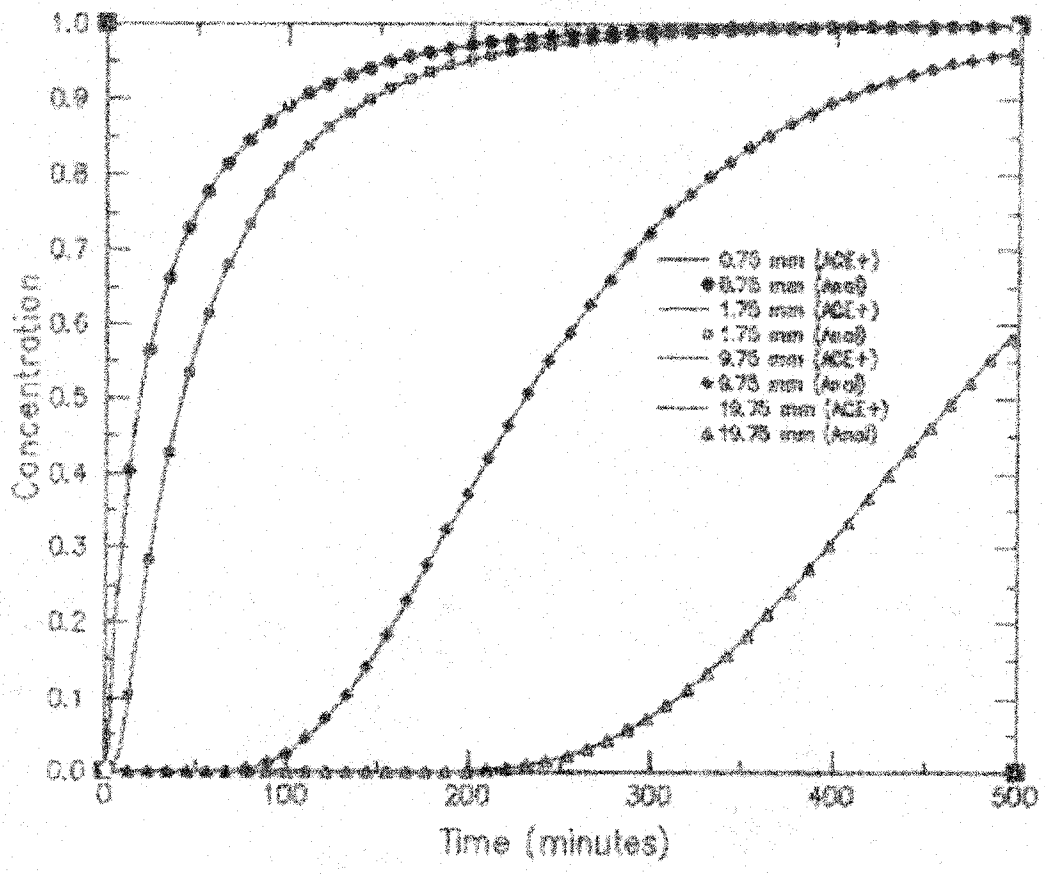

Figure 21: Validation Results from CFD-ACE+ Software (Krishnamoorthy, 2002).

flow near the channel edges properly. The sample section was 100 μm wide, and the beginning of the sample section was at 300 μm from the left side of the channel. The simulation was run for 480 steps for a total time of 45 seconds. The results of the straight section simulation are shown in Figure 22. The difference between the analytical and computed solutions in Figure 22 show an overall magnitude drop of approximately

12.5%. The analytical solution was computed from Equation (22). Note that this graph is not a time dependant graph, but is a cross section of the channel taken at 45 seconds into the solution.

5.2 Standard Turn

The results of investigating dispersion in a turn and supplemental background

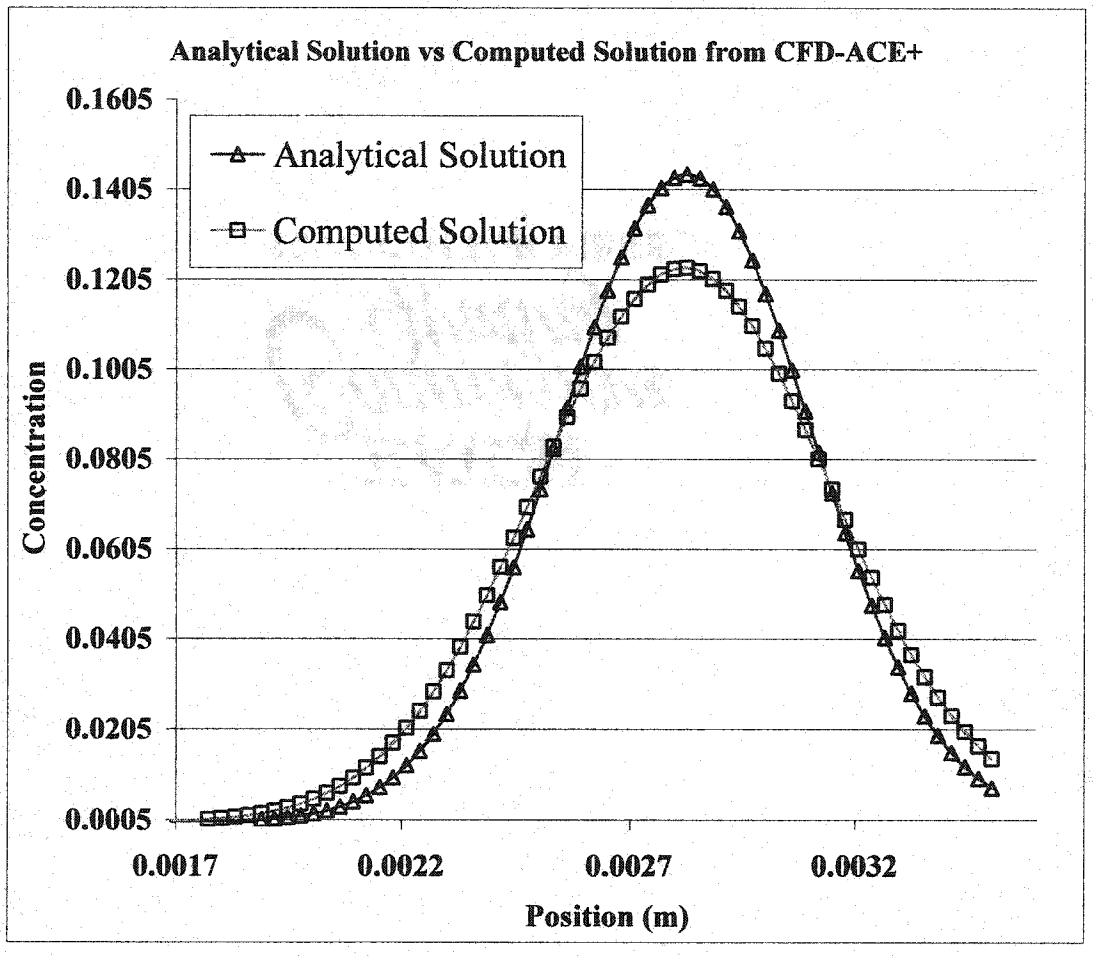

Figure 22: Validation Results from CFD-ACE+ Software and Analytical Solution to Diffusion Equation.

information are now discussed.

5.2.1 Dispersion--Current Literature

Figure 23 shows the relationship between the modified Peclet number versus the normalized variance. As can be seen from the graph, there is a good relationship between the equations (lines) versus the simulated values (symbols) as determined by previous studies. The dashed line represents total variance computed from Equation (29), and the solid line represents the dispersion variance from Equation (30). The triangles, circles,

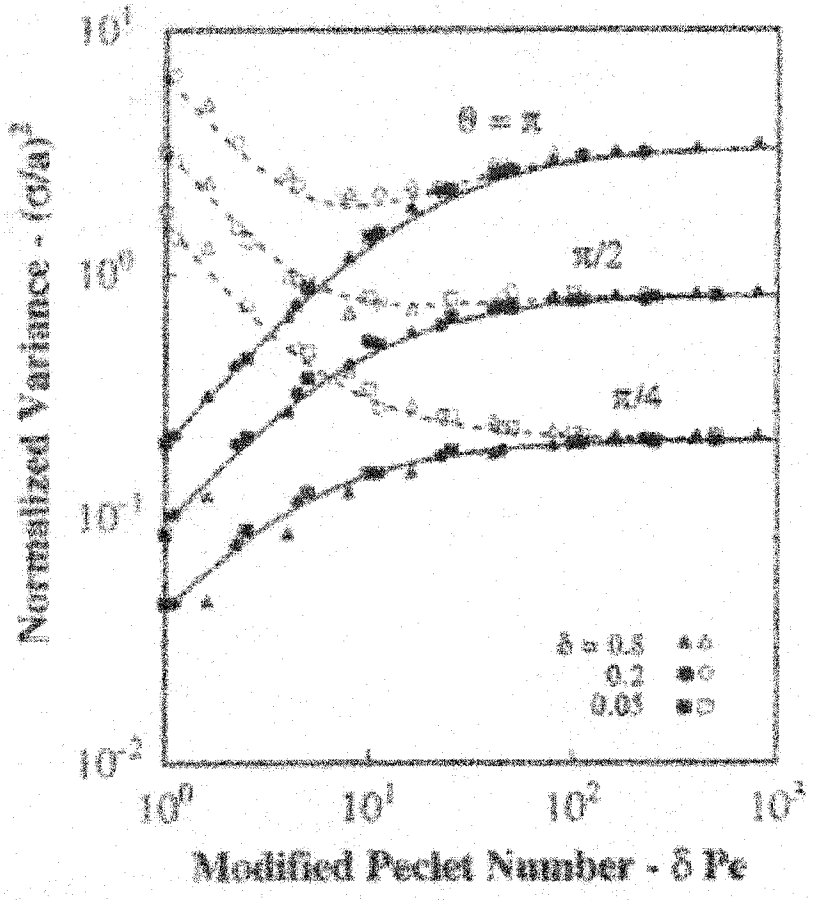

Figure 23: Comparison Between Analytical (curves) and Numerical(symbols) Results from a Monte-Carlo Simulation (Griffiths & Nilson, 2000).

and rectangles represent the simulations done with the Monte Carlo simulations. A close correlation between the analytical solution and the simulation results are based on the width radius ratio, δ are observed.

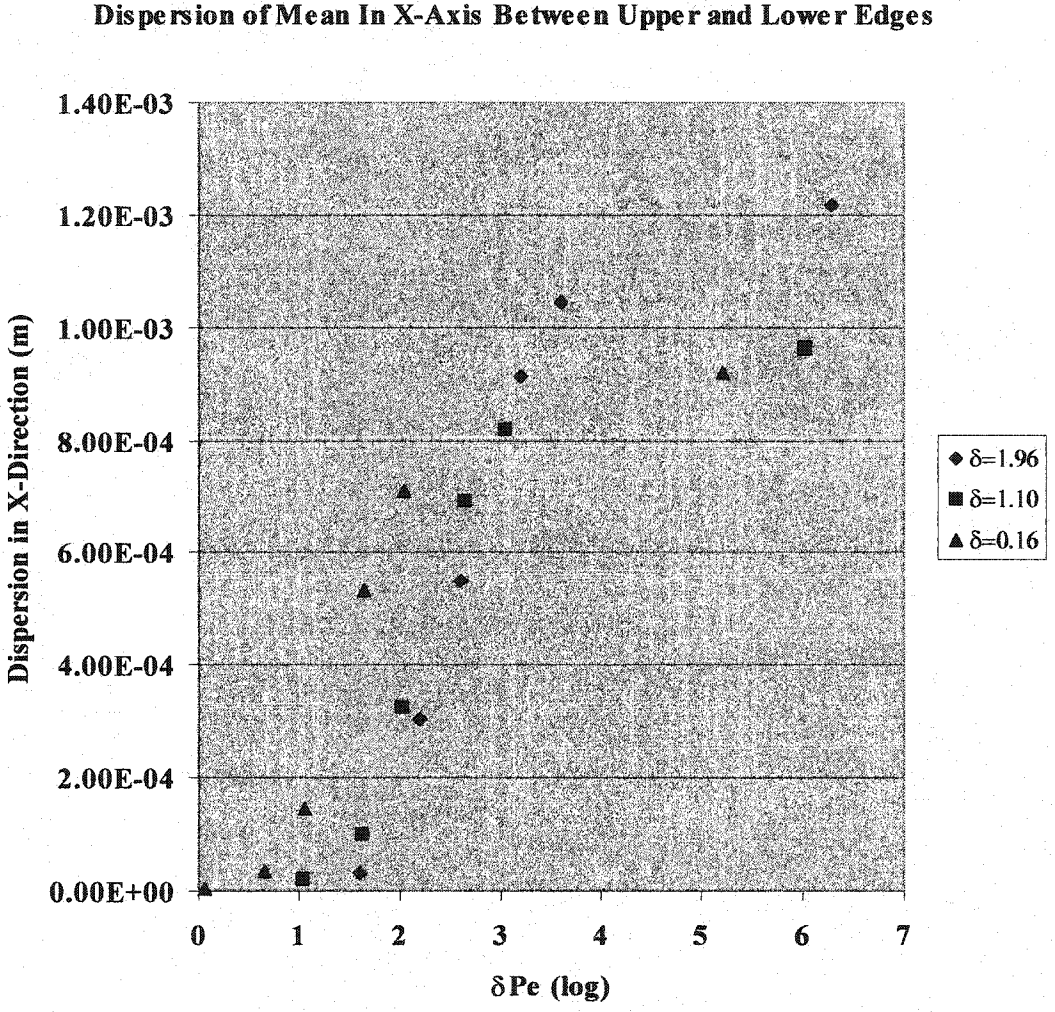

Figure 24: Dispersion of Mean of Sample with Three δ Values.

5.2.2 Dispersion--CFD-ACE+ Studies

Figures 24 and 25 show the dispersion and normalized dispersion variance from the simulations at three different δ values, respectively. There were nine simulations at

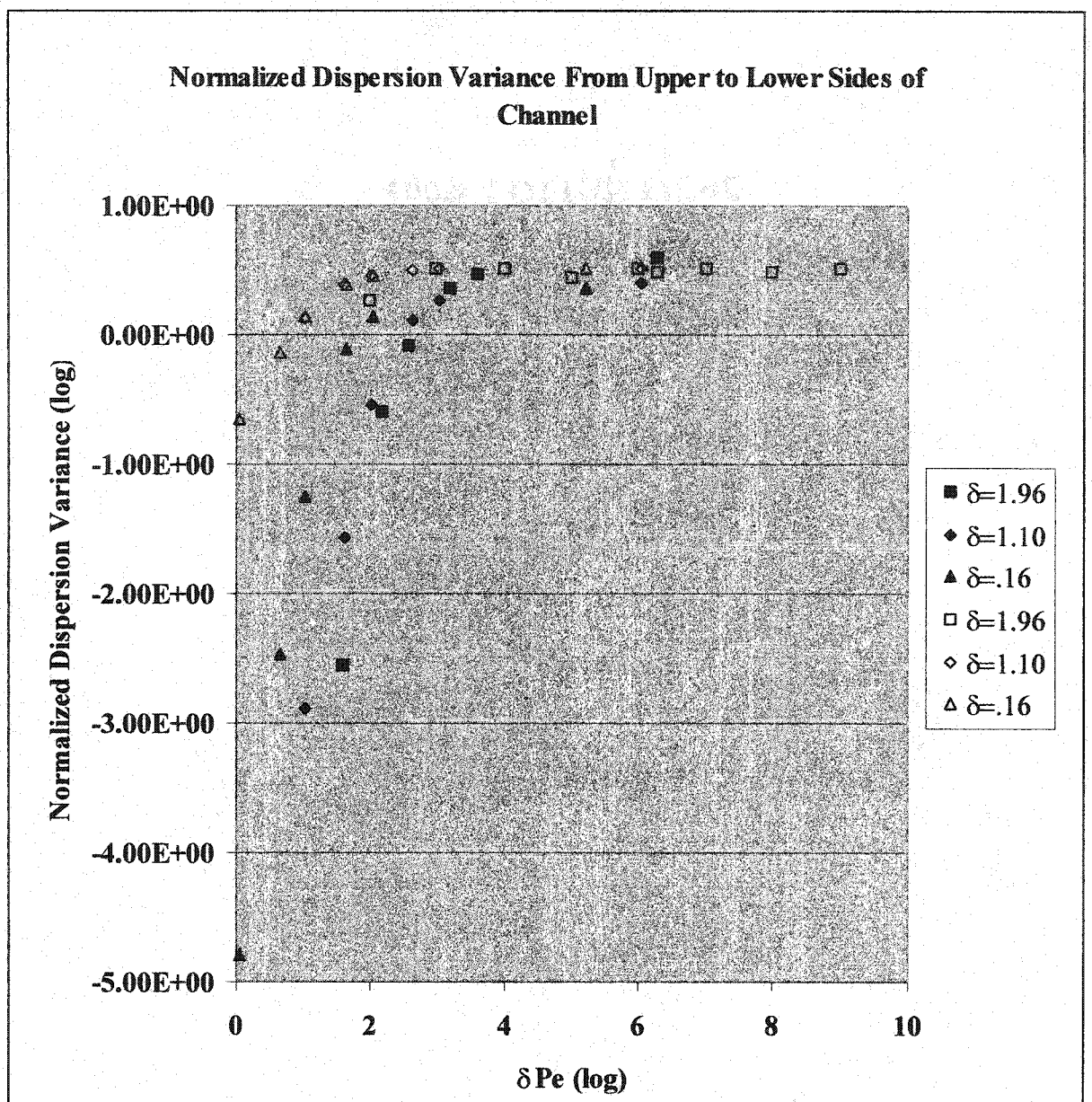

Figure 25: Graph of Rectangular Based Variance and Analytical Variance from Current Literature. (Open Symbols are Computed Values from Equation (30))

the corresponding Peclet numbers shown on the graph. Note that some data points were so close together that they were nearly identical to other values. The geometry conditions for the 27 simulations are shown in Table 1, with nine simulations for each different

radius. On the same graph of the dispersion variance are values from Equation (30), represented by hollow symbols, developed by Griffiths and Nilson. These data points have been identified by "Anal", to represent the analytical values from the equation, where applicable.

Dispersion was calculated from the distance between the means of the upper and lower edges of the channel in the x direction. Each of the points in the graph corresponds to a simulation at different modified Peclet numbers. In these cases, only the simulated values were plotted, and the results of those values are shown in Figure 24.

The residuals of these simulations, corresponding to the leftover error from each time step, were used to quantify the quality of the results from the data. In the first simulations of the turns, the results that made the most sense corresponded to residual errors of 1E-5 after the iterations from each time step were finished. This error was used as a baseline for the first iteration residual when the simulation was run. In the simulations computed for the three different radii, the maximum residual error in the beginning was around 2E-6 for the electric potential and tapered off to around 1E-8 after five time steps. The residual error then decreased 4 to 7 orders of magnitude in an exponential fashion to a residual of 2E-13 +- 2 orders of magnitude. For the concentration error, the maximum value was 2.65E-6, quickly moving down 1-2 orders of magnitude after a few time steps, then exponentially decaying 2-3 more orders of magnitude minimum near the end of the simulation.

5.2.3 Variance--Current Literature

Variance in a turn was studied through two different methods, and plotted against the modified Peclet number. The first was the total variance as Equation (29), to compare with the previous Monte Carlo simulations, and was plotted in Figure 23, normalized to the width, "a". The shapes represent different radius width ratios for the Monte Carlo simulations studied and the dashed line represented the total variance.

Figure 26 shows a chart of the scaled variance versus time ratio as plotted by Griffiths and Nilson. The plotted points correspond to experimental values done by Culbertson et al. The lines represent Equation (29) less the time based variance term "2Dt", and is plotted for two different values for the channel width, "a". The second width, indicated by "a=w-h", is plotted next to the experimental values to show that when the original "a=w" curve is multiplied by a normalization constant, the results of the experiments with the trapezoidal side walls of 45 degrees match the analytical equation less the "2Dt" term. The numbers 38, 47, and 60 represented different channel widths, w, in microns, which are based on previous experimental studies with a channel height of 10 μm (Griffiths & Nilson, 2000).

5.2.4 Variance--CFD-ACE+ Studies

The total variance of the sample after the turn in the three simulated cases from Table 1 is shown in Figure 27. Sample calculations for calculating the variance are shown in Appendix A, using Equation (28). The total number of concentration sample points was 2100, evenly spaced along the channel. The concentration data was sampled

when a majority (>95%) of the concentration of the lagging side had cleared the turn. The results were plotted against the normalized total variance and the modified Peclet number as in the Griffiths and Nilson study, Figure 23. Error for the measurements is expected to be 15-20 percent, based on the additional diffusion due to the iteration

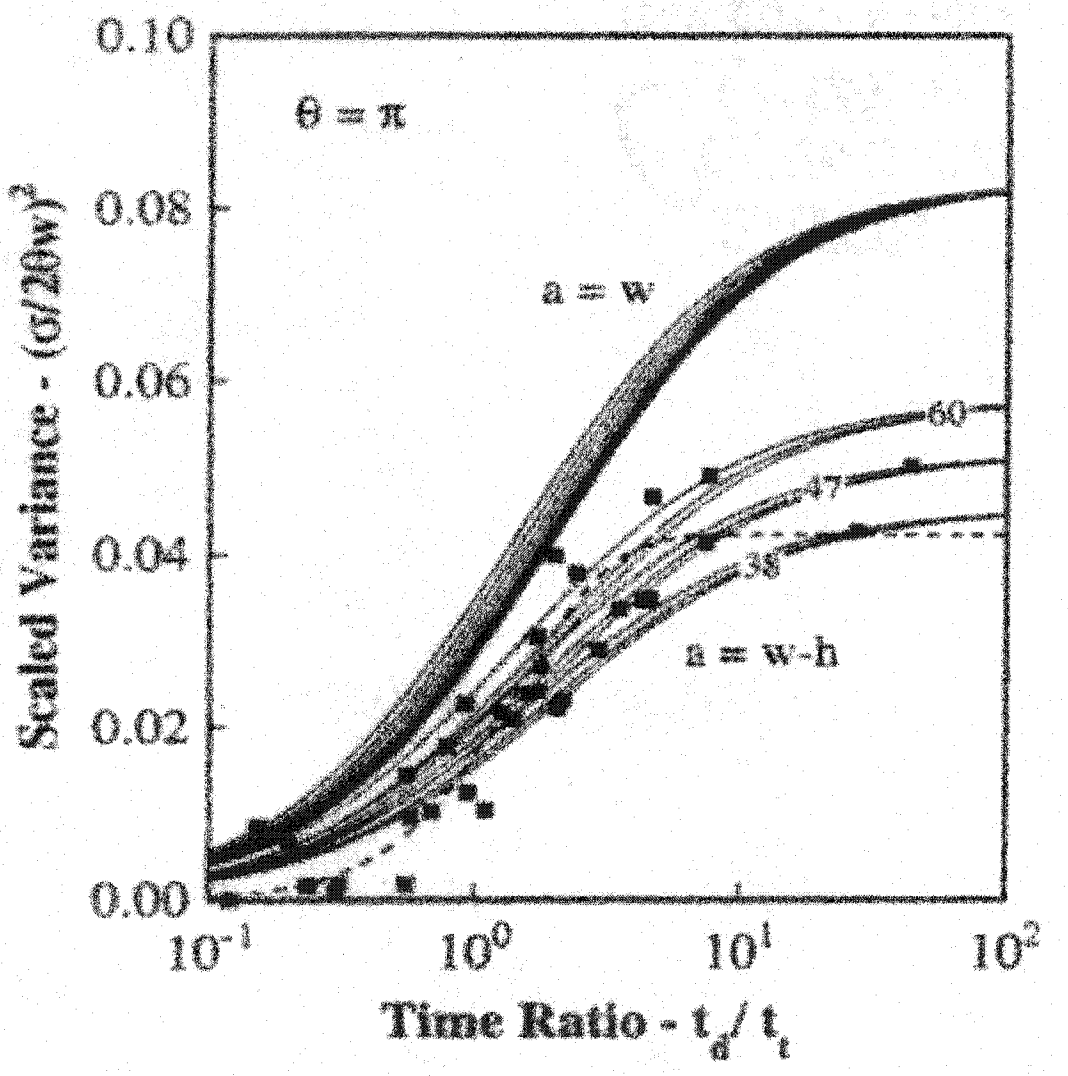

Figure 26: Scaled Variance vs Time Ratio of Experimental (Culbertson et al.--Plotted Points), and Simulated Monte Carlo Method Results.

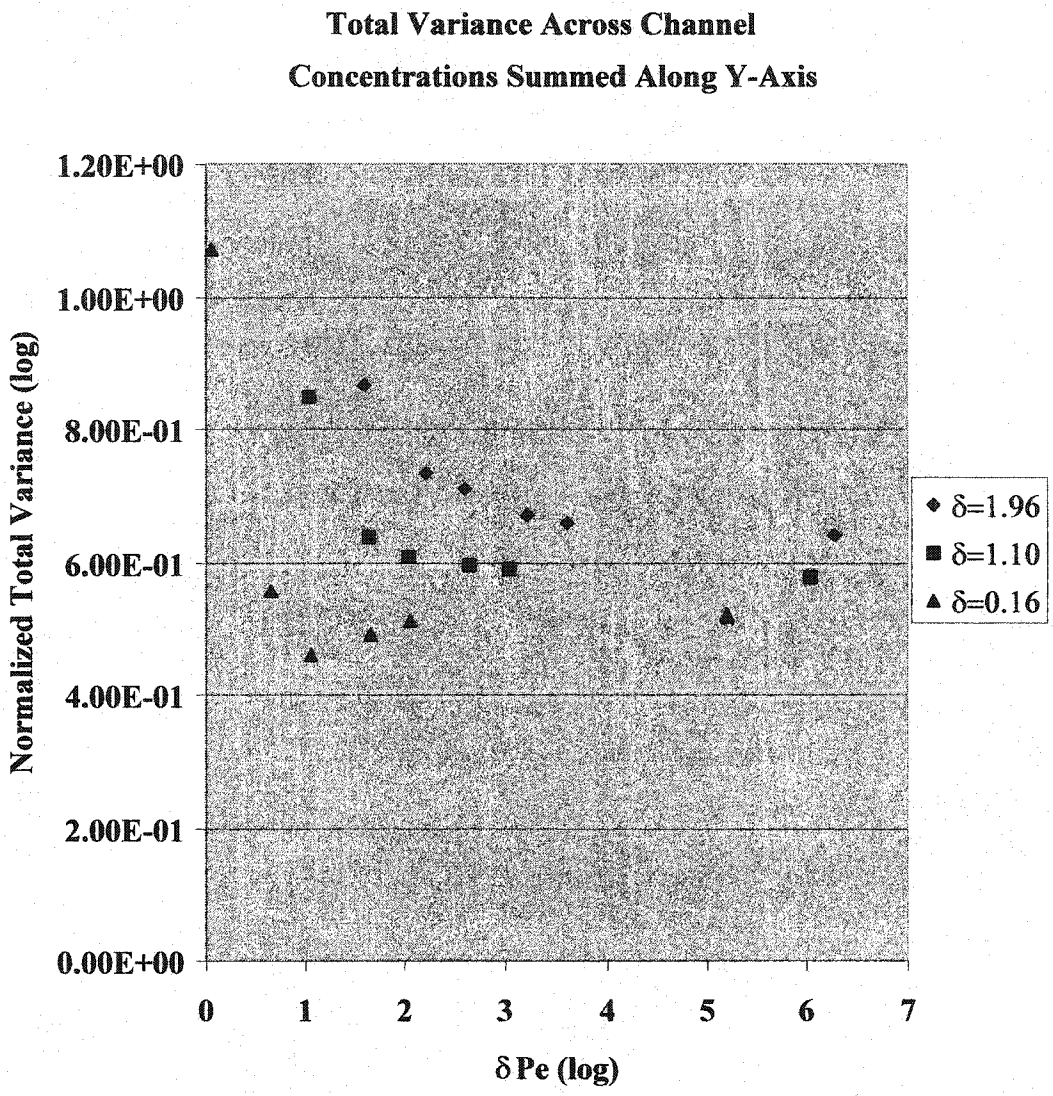

Figure 27: Total Variance of Sample Along Y-Axis For Various δ and Peclet Numbers (See Table 1).

process, as described in the validation section previously.

Figure 28 shows the scaled variance versus time ratio plot of the simulated cases generated by the CFD-ACE+ software. For the scaled variance cases, the estimated variance due to time was subtracted from the total variance, to remove the effects of

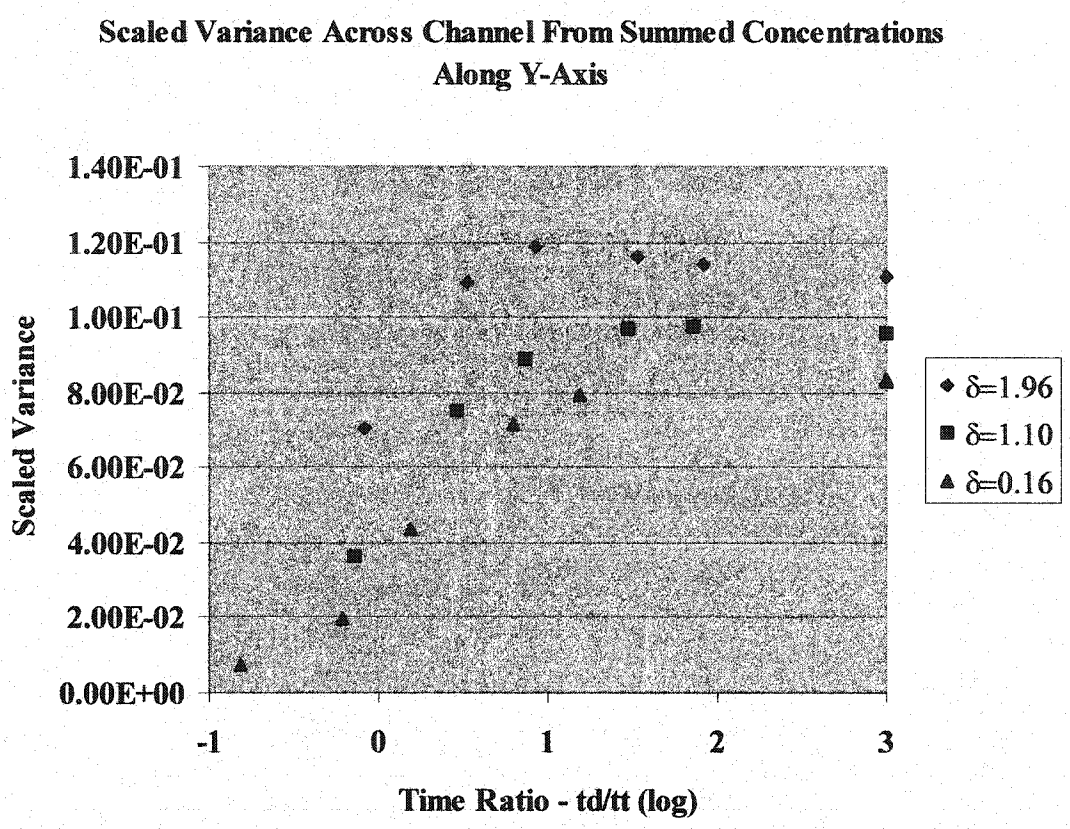

Figure 28: Scaled Variance of Band Along Y-Axis For Various δ and Peclet Numbers (See Table 1).

diffusion and isolate the contribution in the turn. The calculation for the scaled variance and time ratio is shown in the example calculations section.

5.3 Material Change After A Turn

The results of simulations done by CFD-ACE+ and experiments done by Johnson et al., (2001) of the sample after the turn with a different zeta potential on each side of the channel, corresponding to a different electroosmotic flow on each side of the channel are shown next.

5.3.1 Current Literature

Figure 29 shows the results of the plate height versus the electroosmotic mobility

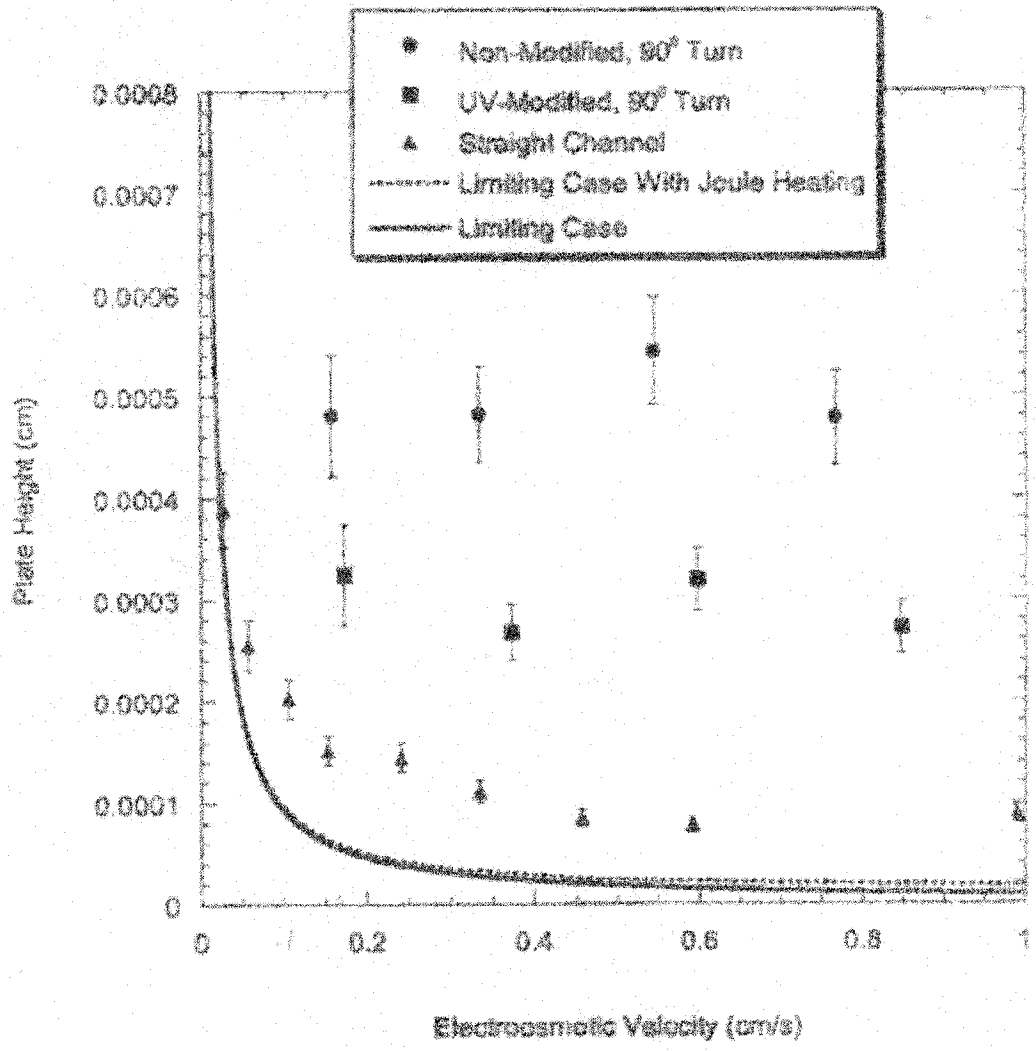

Figure 29: Plate Height vs Electroosmotic Velocity (Johnson et al., 2001).

for the experiments from the NIST study. The figure shows the results of the plate height for the uv-modified, unmodified, straight channel, and limiting cases with joule heating

and without joule heating. Error bars are given for the data retrieved from the experimental apparatus in the figure (Johnson et al., 2001).

Figure 30 shows the converted values of plate height from Figure 29 to an equivalent dispersion change from the leading and lagging edges of the channel. The equation to convert plate height to dispersion is Equation (35) and sample calculations are in the sample calculation section. In Equation (35), H is the plate height, D_{eff} is the effective diffusion rate, u_{EO} is the electroosmotic mobility, t is the time of the measurement, t_0 is the initial start time, and w is the width of the species after the turn. In the same graph are predicted values of the dispersion change due to a 4 percent biased electroosmotic velocity change on one of the sides of the channel. Error bars for the predicted values are included in the figure.

$$H = \frac{2D_{eff}}{u_{EO}} \qquad (35)$$

$$w^2 = 13.139 D_{eff}(t - t_0)$$

5.3.2 CFD-ACE+ Studies

Table 3 shows the range of conditions for the simulations done. The spacing between cells was 22 microns in the x direction and the spacing between cells in the y-direction was variable to have a large density of cells near the surface of the channel to simulate the electroosmotic flow properly.

In the simulations run for the straight channel segments, the maximum residual error for the first few time steps was 1.49E-8 for the concentration and tapered off to

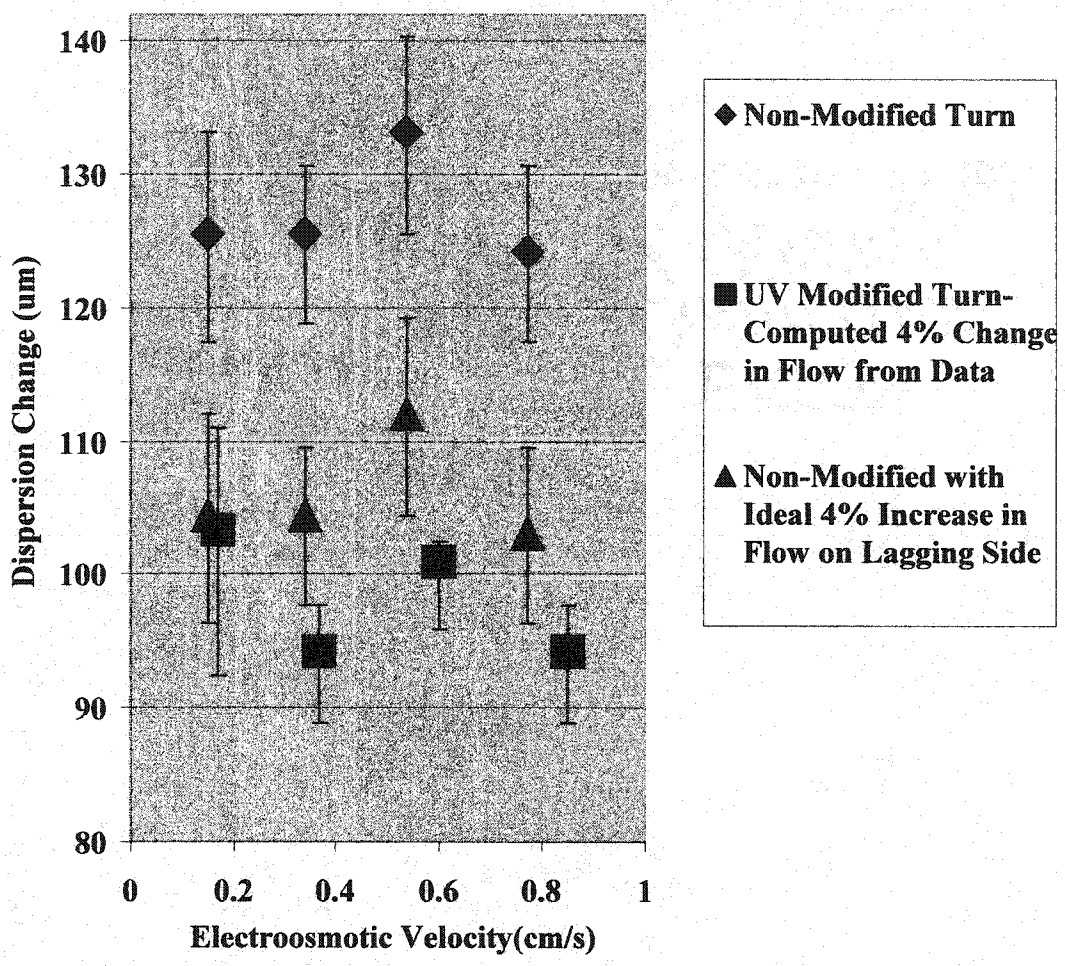

Figure 30: Projected Reduction of Dispersion from 4 Percent Change in Speed.

around 1E-35 exponentially. The electric potential residual started at 8E-16 at the beginning of the simulation, moved up slightly to 7.4E-16 at the end of the simulation, and stayed relatively constant there for the simulations.

Figure 31 shows a graph of the concentration distribution with an electroosmotic mobility ratio (F-ratio) of 1.18. The apparent reduction in concentration magnitude is

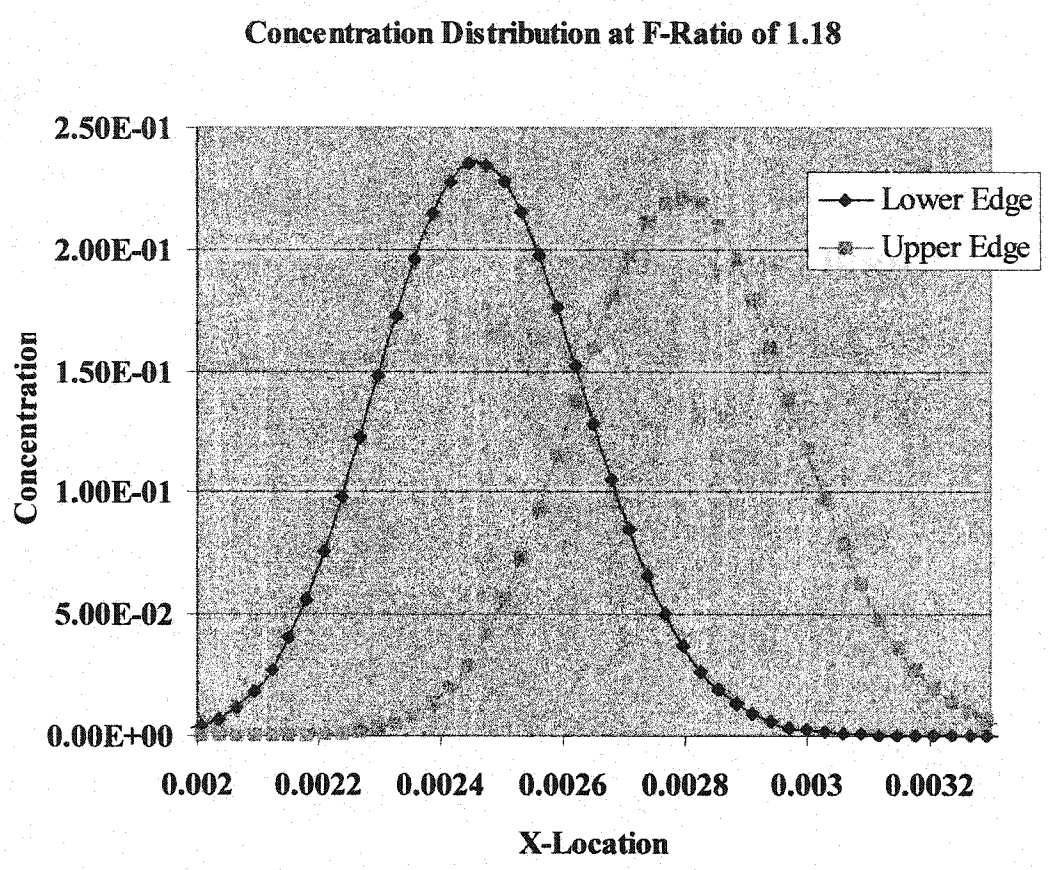

Figure 31: Concentration Distribution Along X-Axis at a Electroosmotic Flow Ratio (F-ratio) of 1.18.

lower by approximately 12 percent.

Figure 32 shows a graph of the local concentration maximum versus the y-axis location in the channel, with the initial concentration being 1. Various F-ratios from 1.02

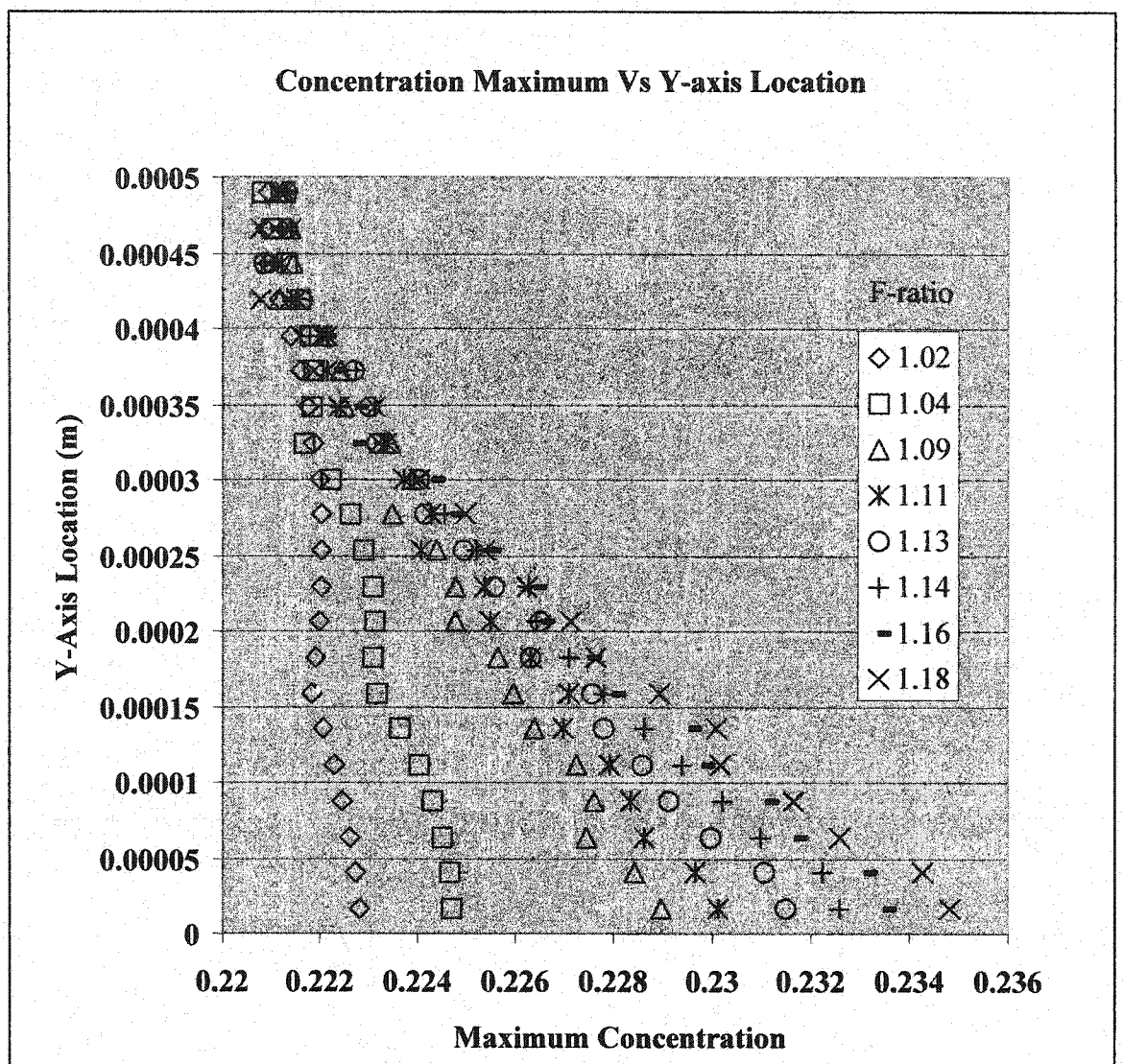

Figure 32: Maximum Concentration vs Y-Axis Cross-Section.

to 1.18 are plotted.

Figure 33 plots the variance of a cross section versus the y-axis of the channel for each of the flow ratios. Figure 34 plots variance versus the y-axis of channel for two additional ratios and diffusion coefficients, different from the small F-ratio studies.

Figure 35 shows a plot of the error of the mean concentration position at the channel walls for the simulated and the predicted values. For the 200 percent difference

in electroosmotic mobility with a maximum Peclet number of 97.5, the worst error was 17.4 percent. For the 471 percent difference, the worst error was 5.3 percent. The maximum error for the 18 percent change in flow was 0.5 percent.

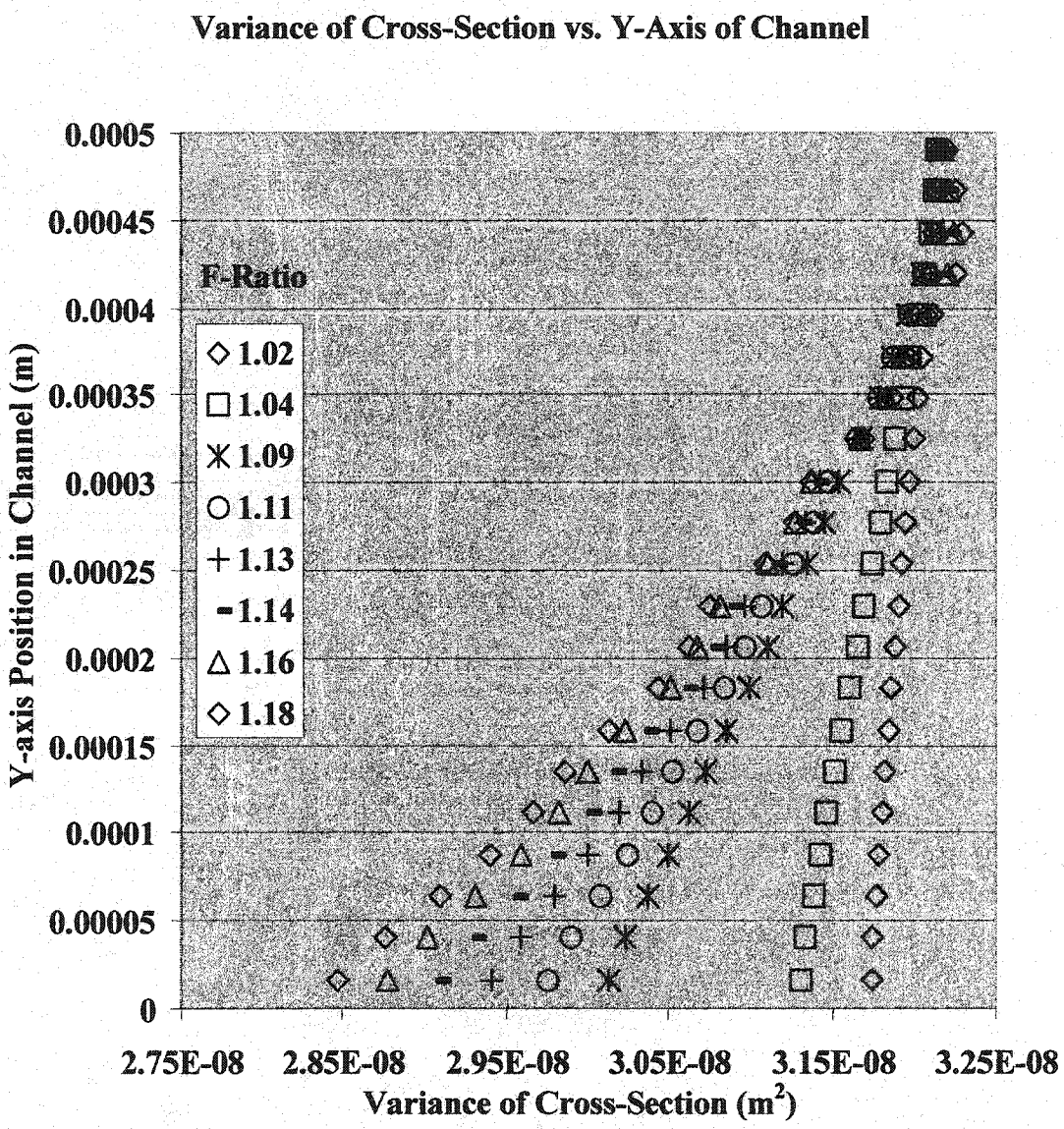

Figure 33: Variance of Cross-Section vs Y-Axis of Channel.

Figure 36 shows percent error of the predicted speed of the mean of the sample versus the simulated mean. The error is plotted for all point across the channel as opposed to on the ends of the channel in Figure 35. Note that at lower Peclet numbers, the error is not just isolated near the ends of the channel, but evenly

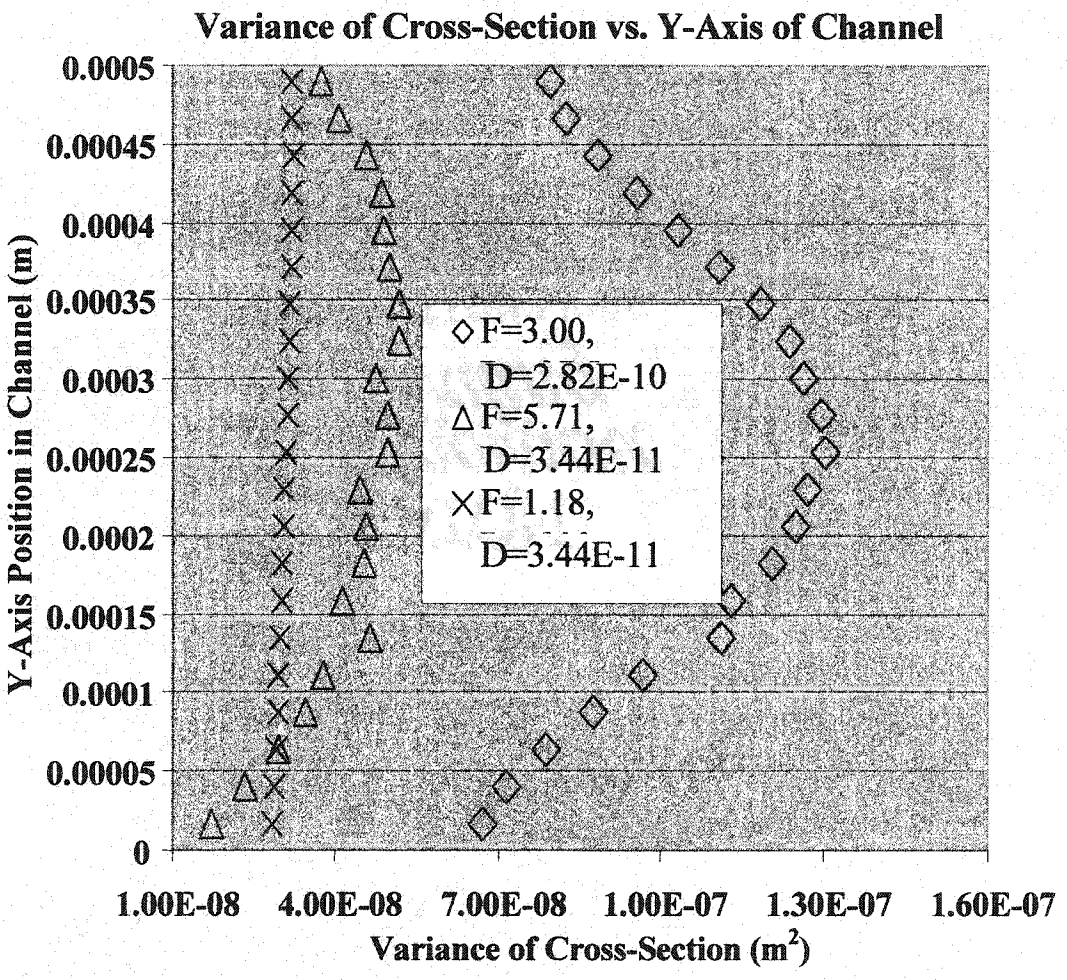

Figure 34: Variance of Cross-Section Vs Y-Axis of Channel for Various Peclet, F-ratios, and Diffusion Coefficients.

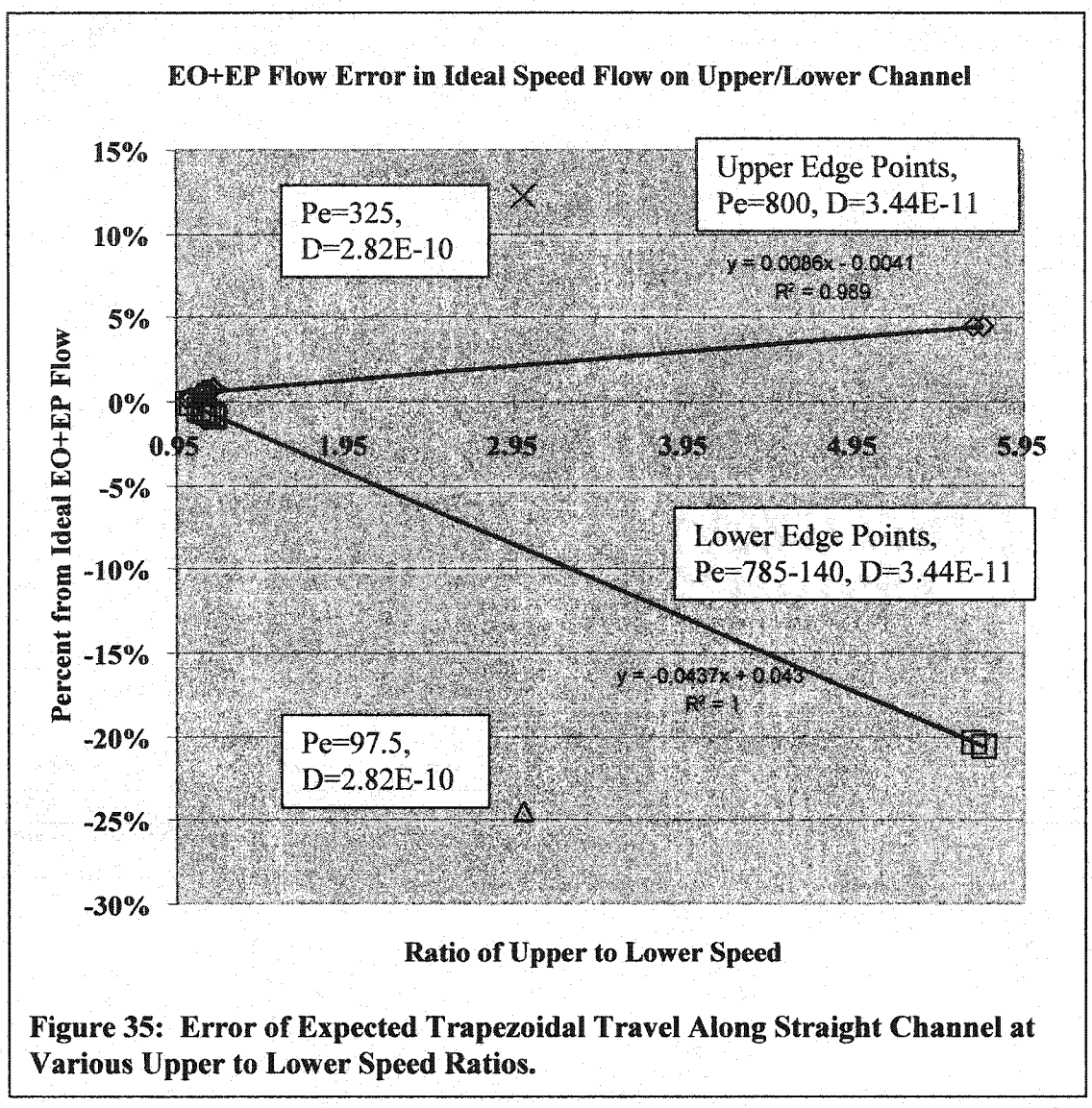

Figure 35: Error of Expected Trapezoidal Travel Along Straight Channel at Various Upper to Lower Speed Ratios.

spread across the channel.

5.4 Electric Field Change in Turn

Table 2 shows the simulation conditions for the three different width radius ratio cases for a step change in applied electric potential. Five different Peclet numbers were

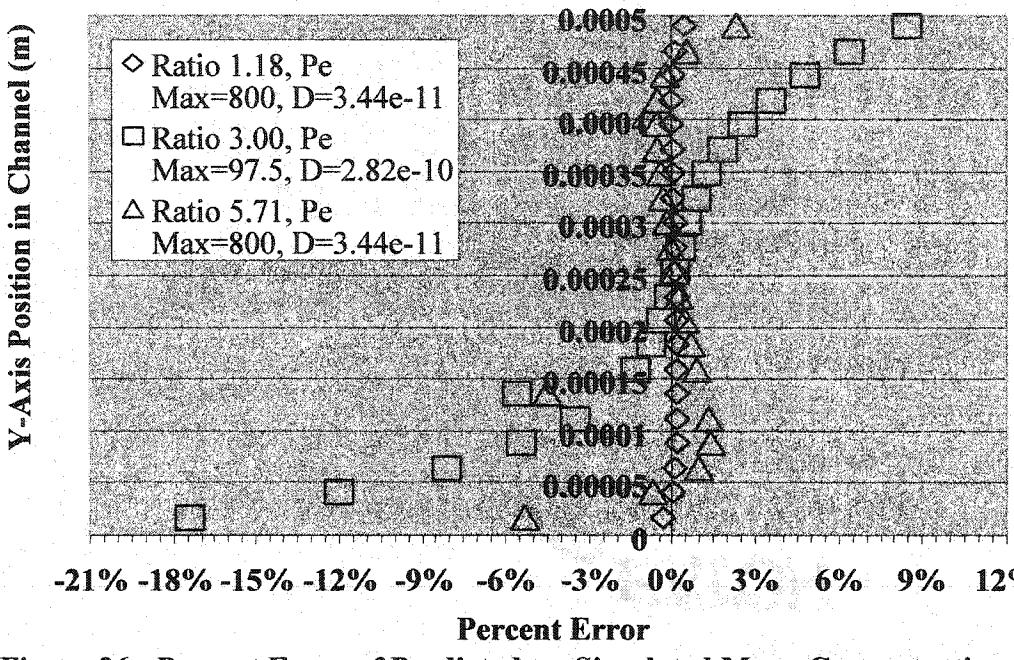

Figure 36: Percent Error of Predicted vs. Simulated Mean Concentration Position for Various EO Mobility Ratios(Lagging Flow is Postitive Percent).

chosen near the "dip" of Figure 23 to simulate what would occur if a step change in applied electric potential occurred in the turn, as shown in Figure 16. Figures 37, 38, 39, and 40 show dispersion, total variance, Normalized dispersion variance, and scaled variance for the simulations with step change in potential along with simulations having no step change in potential. For each of the four figures shown, the Peclet and time ratio values plotted were chosen at the Peclet number for the step change in potential in the turn, not the initial Peclet number of 1000. The time differences for each of the simulations are shown in Table 4, compared to a simulation with no step change in potential.

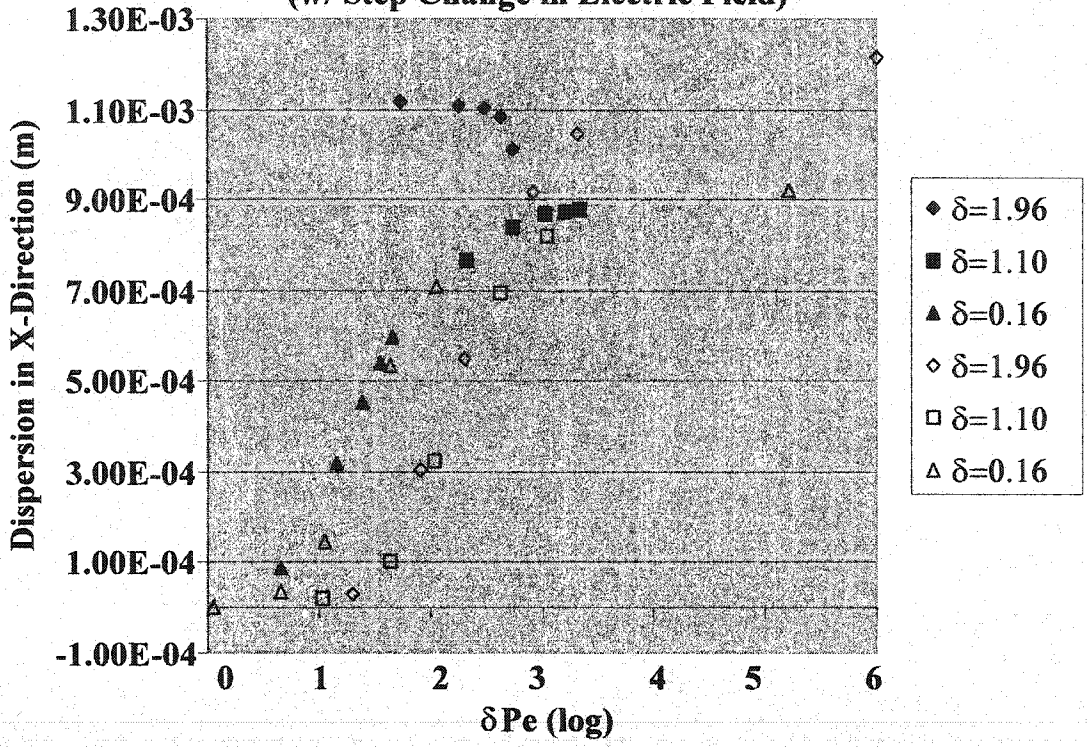

Figure 37: Dispersion of Mean of Sample with Three δ Values with Step in Electric Potential.

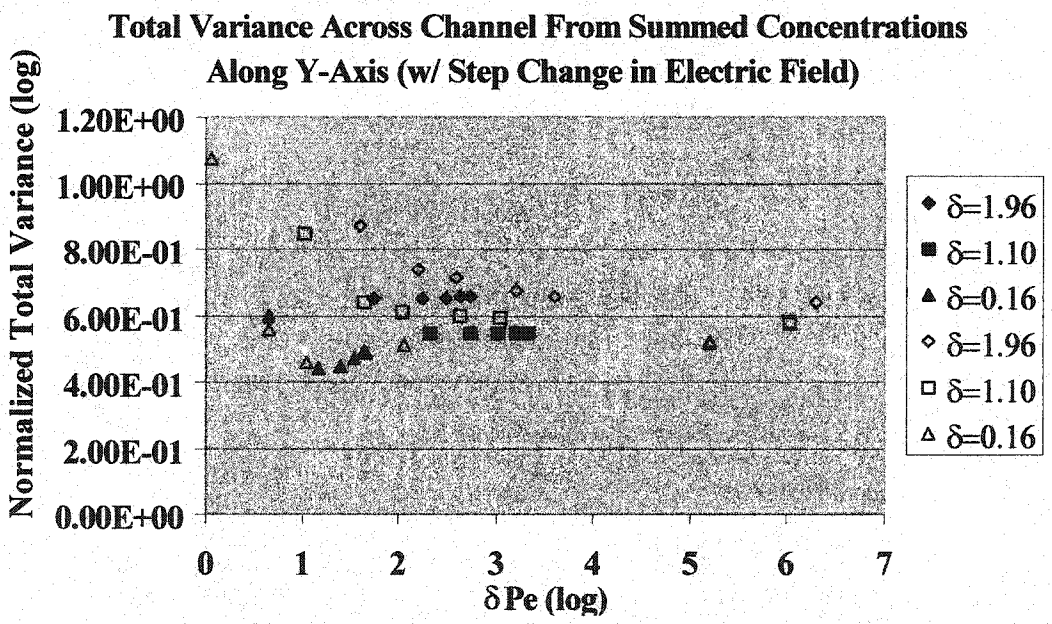

Figure 38: Total Variance of Sample Along the Y-Axis For Various δ and Peclet Numbers with Step in Electric Potential.

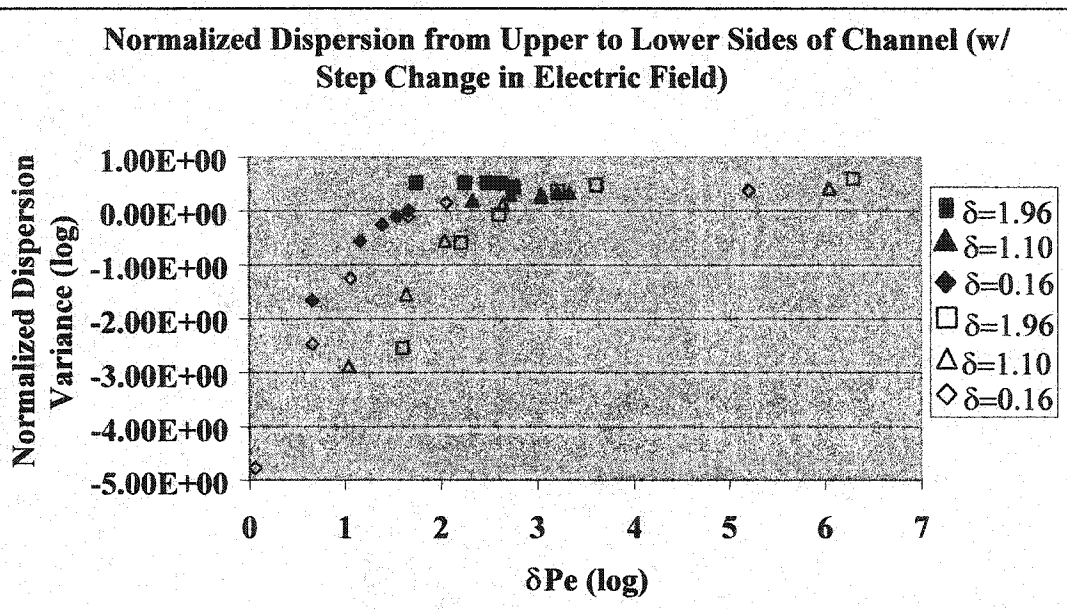

Figure 39: Graph of Rectangular Based Variance and Analytical Variance from Current Literature with Step in Electric Potential.

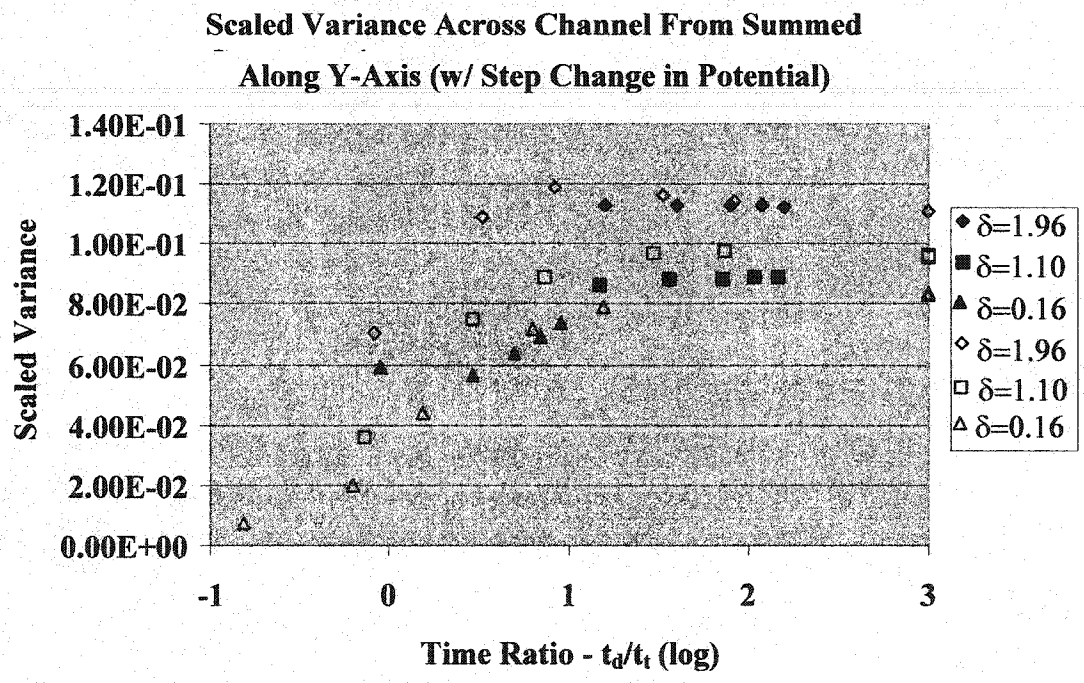

Figure 40: Scaled Variance of Band Along Y-Axis For Various δ and Peclet Numbers with Step in Electric Potential.

6.0 Discussion of Results

The discussion of results is separated into four sections. The first is the validation section. The second is the results of the turn studies with no step change in potential, compared to the previous studies done by other scientists as published in current literature. Third are studies of electroosmotic flow differences from one edge of the channel to the other. Last is the limited control case of a step voltage change rather than a constant voltage throughout the turn with no experimental results.

6.1 Validation of CFD-ACE+ Software

Figures 20, 21, and 22 show the results of various authors in validating the CFD-ACE+ software. In Figures 20 and 21, the results of the simulations closely match the results of the analytical solution to within a few percent. The software is thus validated for the 1-D problem assuming a small enough time step and cell width.

For the studies done here along with the electroosmotic flow tests, some artificial diffusion seems to have crept into the problem, as shown in Figure 22. The apparent error from the analytical solution is around 16 percent for the maximum concentration. The distance error is not affected much, and seems to be less than 2 or 3 percent.

Differences in the two verification studies may be from the number of cells in the travel direction. In Figure 22, there were a number of cells in the x, but also in the y direction, which increased the amount of time to produce a good solution. For comparison, the results from the simulations in Figures in 20 and 21 were done with one cell for the channel width. Thus for the third validation case, there were more

calculations which had no effect on reducing the artificial diffusion from the overall solution.

For the cases using the CFD-ACE+ solution, the order of the residual was similar to the order of the residual for the other simulations. So it is reasonable to assume that the results obtained in the simulations here have some artificial diffusion close to 16 percent.

6.2 Dispersion In a Turn

In the study done by Griffiths and Nilson, the normalized dispersion variance from the simulations seemed to closely match the results from Equation (30). In Figure 18, the largest error is difficult to perceive, but seems to be quite close to the equation developed, with an estimated 20 percent error seen from the equation and the data points.

The CFD-ACE+ chart, Figure 25, shows the same variance in the limit of high modified Peclet number, but it seemed to dive off much more sharply. The reasoning for this is how dispersion is calculated. For the analytical equation, it is not known if the size of the sample was taken into account initially. If the initial sample length was 10 times the length of the arc of the turn, the effects could be quite different due to various mixed diffusion effects. Further, the equation was developed with the assumption of an electric field that was directly proportional to the radius. In the simulations done here, the initial sample size was large compared to the studies of Griffiths and Nilson to reduce initial artificial diffusion from having too few cells with the initial concentration. A narrow sample, with many cells would have required a greater number of computations, reducing the amount of data collected. In the experimented EO flow cases of Johnson et al., the

dispersion was calculated from sampling a cross section across the channel, and selecting a point with a 10/90 percent total concentration ratio rather than the mean, which is a 50/50 percent total concentration ratio. This bias is what separates the mean based variance versus the 10/90 percent method, and when the simulated CFD-ACE+ results are calculated using this method, some, but not all of the values can be made to match Equation (30). This error is larger with larger δ values and is thought to be from the electric field effects in the turn, and the criteria that the equation developed is relevant for δ less than 1, as indicated by the current literature.

6.3 Variance in a Turn

From Figure 23, there is a close relationship between the modified Peclet number and normalized variance as described by the current literature. The error from the simulated values to the equation seems to be mostly positive, and may be due to minor artificial diffusion effects. The error is close to 20-30 percent as described in the graph, closely relating the analytical and Monte-Carlo simulated results for the three δ values. The results from Figure 27 however are different from Equation (29), in that the only δ value that seems to closely match the equation is for δ=0.16. Equation (29) does not seem to apply in the small radius cases, because the equation was originally developed with an assumption that $\delta << 1$ and a constant electric field (Griffiths & Nilson, 2000). The reasoning for this is from artificial diffusion from the numerical scheme and a tendency for the sample to trend toward the inner edge of the turn from a high electric field strength inside the turn. The total variance seems to get larger with small radius but

is constant in the limit where log(δPe)>3, which typically would be the operating range of such a device.

Figures 26 and 28 show simulated Monte-Carlo, simulated finite volume, analytical, and experimental results of scaled variance for a range of time ratios. At first glance, the simulated and analytical results do not seem to match in some places with respect to the a=w graph of Figure 26 and the simulations as shown in Figure 28. This is because the experiments performed by Culbertson et al. were done inside of trapezoidal channels, with a height of 10 μm. As noted in the literature, however there is a scaling factor involved. The scaling factor is determined by understanding that width scaling is linear with Equation (29) at high Peclet numbers. The left hand side of the equation has a 'a^2' but as the walls are trapezoidal for the experimental results, the width should be an average of the width of the channel. The resulting scaling factor is given in Equation (36) below, and when multiplied by the curve 'a=w' in the graph, gives the results for the trapezoidal channels, 'a=w-h', where the quantity 'w-h' is the average width of a trapezoidal channel. As indicated in Figure 26, the dotted line is the results of the equations developed by Culbertson et al., and seems to fit the simulations and trapezoidal channel experimental results closely. In Figure 28, the best fit to previous studies seems to occur with a δ value of 0.16, as in the previous normalized total variance case.

$$(a = w\ curve) * \left(\frac{a-h}{a}\right)^2 = (a = w - h\ curve) \tag{36}$$

From a design standpoint, the more important criteria for discussion is the total variance, as the scaled variance removes the effects of diffusion over time. The scaled

variance is used here to compare to experimental data. In Figures 23 and 27, the best range of operation seems to be in the positions with condition $\log(\delta Pe)>3$. The reasoning for this is from predictibility, as for $\log(\delta Pe)>3$ the total variance does not change. The dispersion here is a maximum, but this is simply a trade-off of having a large total variance. The upper limit of practical application as $\log(\delta Pe)<4.5$ is from diffusion due to Joule heating, giving a latitude of 1.5 orders of magnitude to work in without worrying too much about diffusion effects.

6.4 Electroosmotic Flow Change

From Figure 30, it is evident that there is some relationship between the predicted dispersion from the unmodified turn and the modified turn cases. One of the data points fit very well when assuming the flow at that level was linear, but the three others seemed to be on the border of error. It is not known whether this error was from wrongly assuming a 4 percent change in flow average or other effects. As noted in the experimental cases (Johnson, et al., 2000), the electroosmotic flow from modified to unmodified sides of the channel was probably greater than 4 percent due to the difficulties in measuring a 'change in flow' but gives no indication as to how much. They note that this was partially from problems with measuring the dispersion from a volume ratio standpoint of 90/10 along the edges of the channel, as discussed previously. The predicted points plotted should then be closer to the actual values assuming a trapezoidal flow velocity. One other interesting thing about Figure 30 is that the distance between the unmodified turn points versus the modified turn points, seems to be nearly the same

distance for the three points of higher EO velocity. This reinforces the assertion that dispersion change regardless of the average electroosmotic velocity is constant and trapezoidal in nature.

The results from the CFD-ACE+ simulations show some interesting results. For a large Peclet number, the maximum concentration seems to be similar across the channel. The concentration is reduced by approximately 8 percent across the channel, at F=1.18, as shown in Figure 31. The variance of the cross section across the channel also counter-intuitively seems to be smaller at the slower edge of the channel, as shown in Figure 33. There could be several reasons for a smaller variance, with the most logical being the combined convective and diffusive force vector on the fluid causes the concentration to be 'compressed' together near the slower end. One of the reasons for this may also be from the assumptions on how the variance is calculated. Take the example of variance in a 1-D fashion. In the case of variance related to diffusion, the term '2Dt' represents the variance from the solution to the 1-D diffusion equation. For a differential EO flow, the slower end separates from the faster end, the 1-D assumption no longer applies as there is now some 2-D diffusion occurring. Thus the variance from diffusion is a little more than 2Dt, with the limit of 2-D variance being 4Dt. Figure 34 shows how the variance in the center gets considerably larger as the average Peclet number gets smaller.

Figure 35 shows that there seems to be some linear relationship of the error at the edges of the channel at various F-ratios and Peclet numbers when the diffusion constant is held at a particular value. This suggests that the trapezoidal velocity profile may need a correction factor, which could be solved by a total solution of the 2-D diffusion equation

analytically with electroosmotic flow. The error here however is notably small (<1%) for a small deviation in EO flow, and for most engineering applications, this 1 percent error would most likely be "in the noise of the error" and could be relied upon under many circumstances. Note that this assumption is at a fixed time period and the error may be larger and exponentially dependent on time. A more detailed analytical analysis will determine if it is linearly dependant or exponentially dependant.

Figure 36 shows how the position error from a low Peclet number can be significant. But for a high Peclet number, with F=5.71, the error across the channel is less than 10%, and for most purposes assuming a trapezoidal profile could be relied upon if needed. The graph also indicates a characteristic "S" shape, which may be dependant on a hyperbolic function of some sort. It is evident here, however, that the simulations show that for large Peclet numbers, the trapezoidal flow profile is accurate to within 10 percent for at least a Peclet number of 800 and F=5.71. It should be noted here again that the zeta potential and Debye-Huckel length are small in comparison to the channel width, and this is one of the conditions for this linearity in flow.

6.5 Electric Field Change

Dispersion from a step change in electric field showed some curious results. For the small δ case, there seemed to be little change in dispersion from the change in electric field. For large δ however, the step change in electric potential seemed to increase the dispersion from the turn. One explanation for this could be because of the sample size as it enters the turn. For small Peclet numbers, with no step change in electric potential, the sample length is quite large in comparison to the size of the turn before it enters the turn

regardless of the step change in e-field, and so the effects of a small δ have little effect. In the case of the step change in potential with large δ, the sample is considerably smaller when it enters the turn at a high initial Peclet number as compared to a low initial Peclet number, and so the effects of dispersion are more apparent.

The most interesting thing about the electric field change in the turn is the effect on the total variance. Figure 38 shows how in the simulations the variance is reduced some, with the most reduction coming from the smallest radius, and almost no change for the case of the largest radius. In the large radius case, slowing down the sample in the turn only adds to the additional diffusion of the problem, as the time to traverse the turn is much longer than for the smaller radius cases. For the small radius case, the reduction is thought from a mixture of effects, partly from the sample size in relation to the turn, and partly the time-based effects. One interesting thing to note is that for scaled variance, there seems to be a small percent reduction for most of the points tested, with exception to δ=0.16. The scaled variance there seems to cross the curve of the scaled variance with no step change in electric field. An obvious explanation for this could be from how scaled variance is calculated. With a step change in potential, the time to diffuse is less, so the scaled variance is larger than it really is.

6.6 Electric Field Effects

The basic analytical model developed by Griffths and Nilson, and Culbertson et al., assumes that the electric field in the turn is linear with the radius. This is not the case with a large δ-ratio, and the electric field in the turn can be quite large in the corners of

the beginning of the turn. Figures 41 and 42 show the magnitude of the electric field at a cross section of the turn with contour lines for δ=1.96 and δ=0.16. In the figures, the effects of the electric field in the inner edge of the turn are much larger with a small radius than a large one, as the electric field is closer to 1/r rather than to a proportionality constant. This 'cornering field effect' is less with a large radius as the field is proportional to a constant. This difference in field strength in the corners is very likely the reasons for an uneven cross-channel concentration distribution as described by Culbertson et al. in Figure 2. This would also explain the slightly different curves for large δ in comparison to $\delta > 1$, and the equations developed by those authors.

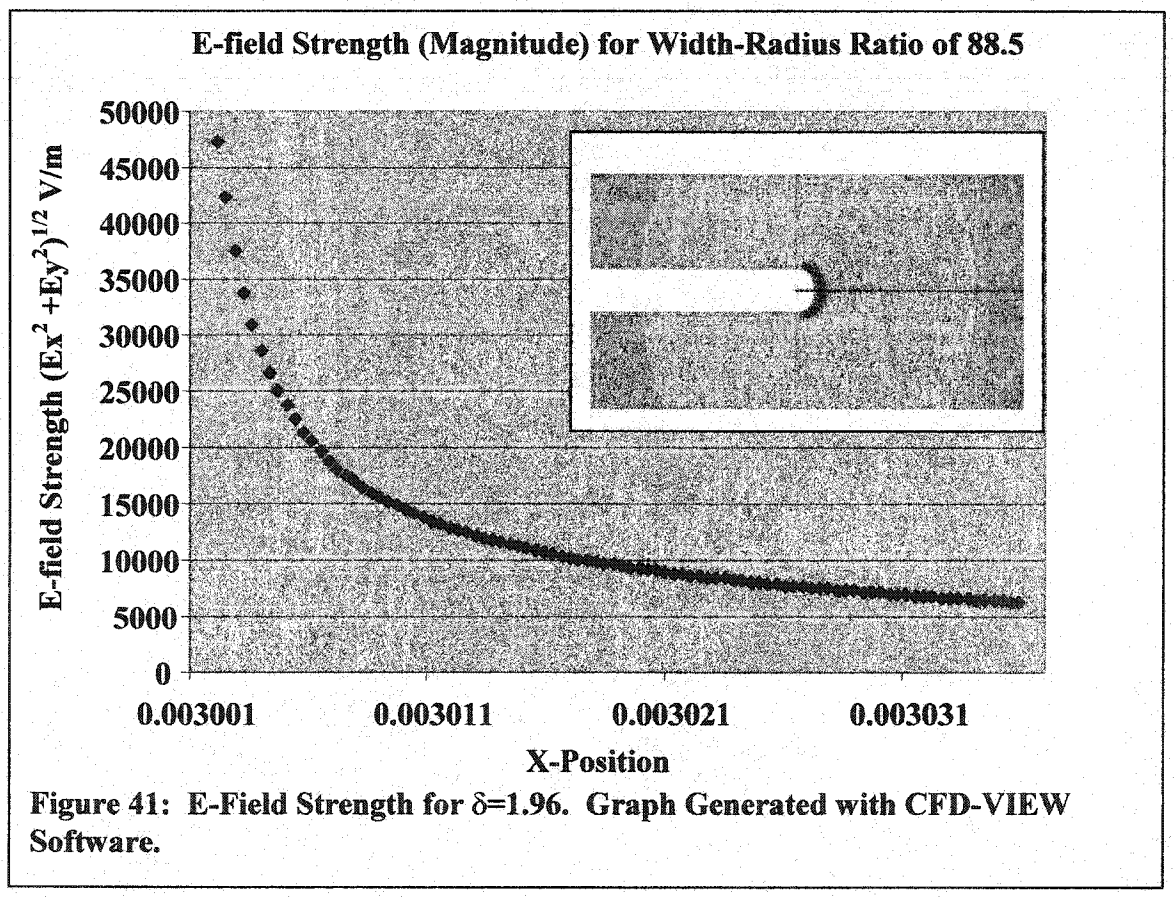

Figure 41: E-Field Strength for δ=1.96. Graph Generated with CFD-VIEW Software.

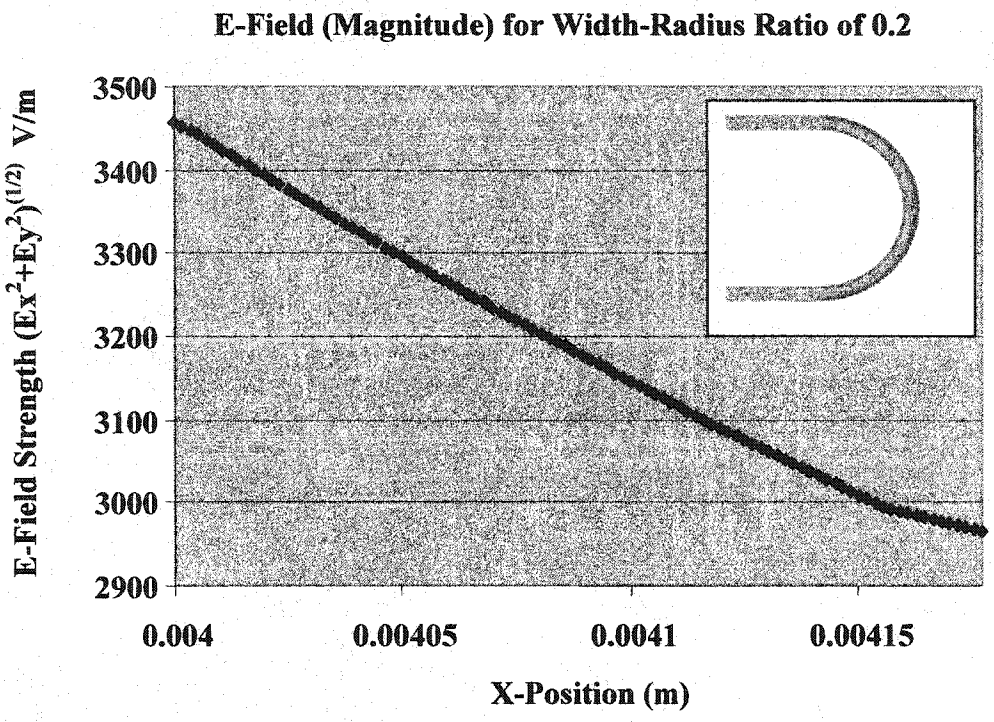

Figure 42: E-Field Strength for δ=0.16. Graph Generated with CFD-GEOM Software.

6.7 Dispersion Comparison

Comparison of the different methods indicates that for dispersion, it is better to let the sample traverse the turn with no electric field change when compared to the step change in electric potential for the points indicated in the charts. This conclusion is supported by the simulated results from the CFD-ACE+ software, but has no experimental supporting data to compare with. Thus it cannot be generalized upon to say that an electric field change will always affect the output in this manner. A more thorough analysis would require that the timing of the step change in potential in the turn be spread out to some range of values where the change occurs some time inside and outside the turn. However, given the experimental, analytical, and supporting data for the

no-electric field method, it can be concluded that the range of modified electric field numbers indicated in Figures 37 and 39, it is probably better not to use this particular electric field control method to reduce dispersion.

6.8 Variance Comparison

Reduction of variance seems to be possible through a step change in electric potential as indicated in Figures 38 and 40. The apparent reduction seems to affect the problem the most for large δ and small δPe, but more simulated data is needed to extrapolate for lower values outside of the ranges simulated. In cases for high modified Peclet number it may be extrapolated to the limits for each of the different δ however, as the convective forces in the problem outweigh the diffusive forces. Thus variance reduction is possible, as a reduction in the time to travel the turn does reduce the effect diffusion has on the problem, and less diffusion implies a smaller variance entering the turn. Thus this method isn't particularly useful as in most cases as the objective is to separate as quickly as possible for a high throughput.

6.9 Sample Size

The sample size in comparison to the inner turn diameter seems to have some impact on how the sample traverses the turn, but only at large δ. When the sample enters the turn small in comparison to the radius, the effect of dispersion seems to overwhelm the sample, and a much larger dispersion results, as indicated in Figure 37. When the sample enters the turn small in comparison to the radius, the sample seems to fall in line with the characteristic curve developed by Griffiths and Nilson, Equation (29).

7.0 Conclusions/Contributions

Two methods have been analyzed to understand the phenomenon of reduction of variance and dispersion of a sample fluid in a microchannel turn. Varying Peclet numbers and width-to-radius ratios were involved in the study. The results show that the equations developed by Griffiths and Nilson, and Culbertson et al., are useful in anticipating the dispersion and variance after the turn for large radius and with a proper scaling factor for different turn cross-section. Further, the equations developed by those authors do not render witn reasonable accuracy in the case when δ is 1 or more, as confirmed by the simulations done here and as discussed in the literature. In the case of very low modified Peclet number ($\delta Pe < 1$), the simulations and the supporting literature indicate that diffusive forces overwhelm the problem, and the resulting variance approaches that of the variance due to diffusion only, that is 2Dt. In the case of very high modified Peclet number ($\delta Pe > 3$), the results seem to be dependant on the radius only for high modified Peclet numbers, and range from a normalized total variance of 6.2E-1 to 5.0E-1.

Application of the specific step change in electric potential method just before the turn has the effect of increasing the dispersion but reducing the variance for the simulations studied, when compared to no method change. The reduction of variance depends on δ, and is larger for a large δ and small δPe. For a step change to δPe greater than 3, a reduction in variance seems to be negligible however, as the convective forces

are significantly larger than the diffusive forces. For very low δPe as indicated in Figures 35 and 36, more data is necessary to determine whether an affect will occur.

Simulations and experiments prove that biased zeta potentials on channel walls in rectangular channels with high Peclet numbers result in a flow that is trapezoidal in nature. This profile is valid even for cases where the electroosmotic flow is up to 5.7 times faster than the slower side for rectangular cross-section channels, with an error of only 2 percent. Thus the dispersion can be described as linear in these cases, and Equation (30) can be used in designing an F-ratio that compensates for any dispersion which occurs in a constant radius turn.

7.1 Summary

Variance and dispersion after a microchannel turn have been shown to be nearly constant after microchannel turns at high modified Peclet numbers greater than 1000 for small and large radius turns. The variance varies only by 20 percent and range from a normalized total variance of 6.2E-1 to 5.0E-1.

Application of a step change in potential just before the turn has the effect of reducing the time based variance when the Peclet number is initially very high. This reduction is negligible when the modified Peclet number is greater than 3 however.

A material change after the turn, when used to change the zeta potential on opposite walls of a channel, has the effect of a nearly trapezoidal flow profile after turn, with small error at high Peclet numbers (>800).

The conclusions above can be summarized and used to design turns for specific applications. The most promising and useful conclusion is adjustment of the

electroosmotic flow after the turn. The constant nature of the dispersion after the turn suggests that a static design will fix most of the dispersion problems after the turn.

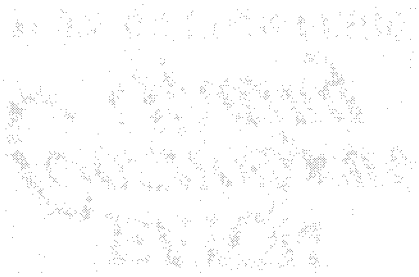

8.0 Recommendations of Future Research

The dispersion and variance results here indicate some dependence on the sample size to the turn size when the electric field is strong at the inside edge of the turn. An analytical solution that accounts for the radius in the solution would provide the most accurate information for conditions when $\delta > 1$ in that case. The model should include the width of the sample and the proper initial conditions of the problem, such as a square sample distribution or a Gaussian sample distribution. This model would provide the most generalized information, however it will be difficult to implement because of the number of variables involved. An experimental or simulation-based approach may be the best approach, as in most engineering applications the number of complexities in deriving an analytical solution are numerous.

Studies based on simulations of an opposite sided turn after the first will provide more design information to use for designing a device, as the information here does not suggest what will happen after a turn designed in the opposite direction. Current studies show that a reduction occurs, but it is not 100 percent removal of the variance. Time based diffusion is the likely problem here, as well as the shifting to the leading side of the sample after the turn.

The distribution profile of the sample as it travels down a straight channel with varying diffusion constants and zeta potentials on opposite sides of the channel would be a good study that would be simple and reliable for use in many engineering applications. The effects of this problem have been touched upon, but more information is needed for the larger diffusion constants and lower Peclet numbers. A more time-based study of

error would also be useful, to see if the error over time is linear, or some other function of time. The effects of a step change in zeta potential should also be included, to see if a large step change causes any strange velocity fields at the surface of the channel or in other areas.

For the electric field changes, the results here gives some preliminary information regarding what could happen in the case of a step change in electric potential, but experimental results and testing is necessary, with sensors, a computer, and other apparatus to determine if the field can even be controlled in the turn. The switch time in the turn is a matter of 0.5 of a second for one of the high Peclet number cases, and some very expensive hardware would be necessary to control that system with a good degree of accuracy. Other time-dependant voltage functions could be tested, but control of the sample as it enters the turn would first need to be demonstrated before any complex time dependant functions were tested.

The three dimensional version of this problem would be interesting to study, as the experimental data compared here was with a trapezoidal channel. In those cases, three-dimensional diffusion effects would be seen, rather than two-dimensional diffusion effects, and may change the curves established here somewhat. As discussed before, the problem would be excessively difficult to generalize, and it would be better to simulate or experimentally characterize each design on a case-by-case basis.

References

Anderson, Dale, et al. (1984). *Computational Fluid Mechanics and Heat Transfer* (pp. 10-80). Hemisphere Publishing Company.

Anonymous. (2001). CFDRC User Manual.

Anonymous, (2001). CFDRC Module Manual.

Camilleri, Patrick. (1998). *Capillary Electrophoresis: Theory and Practice, 2nd Edition* (pp. 1-200). CRC Press, LLC.

Culbertson, Christopher T., Jacobson, Stephen C., & Ramsey, J. Michael. (1998). Dispersion Sources for Compact Geometries on Microchips. *Analytical Chemistry, 70,* 3781-3789.

Cussler, E. L. (1997). *Diffusion: Mass Transfer in Fluid Systems.* Cambridge University Press, New York.

Gebhart, Benjamin. (1993). *Heat Conduction and Mass Diffusion.* McGraw-Hill.

Giddings, J. C. (1989). Harnessing Electrical Forces for Separation. Capillary Zone Electrophoresis, Isoelectric Focusing, Field Flow Fractionization, Split-Flow Thin Cell Continuous Separation and Other Techniques". *J. Chromatography, 21,* 480.

Griffiths, Stewart, K, & Nilson, Robert, H. (2000). Band Spreading in Two-Dimensional Microchannel Turns for Electrokinetic Species Transport, *Analytical Chemistry, 72,* 5473-5482.

Johnson, Timothy J.; Ross, David; Gaitan, Michael; & Locascio, Laurie, E. (2001). Laser Modification of Preformed Polymer Microchannels: Application To Reduce Band Broadening around Turns Subject to Electrokinetic Flow, *Anal Chem, 73,* 3656-3661.

Jorgenson & Lukas. (1981). Zone Electrophoresis in Open Tubular Glass Capillaries: Preliminary Data on Performance, *Journal of High Resolution Chromatography, 4,* 230.

Krishnamoorthy, S. (2002, April 5). Simulation of Sample Transport in Microchannels: Validation Studies & Model-Setup Guidelines, CFD Research Corporation.

Manz, A. (1993). Planar Chips Technology for Miniaturization of Separation Systems: A Developing Perspective in Chemical Montoring, *Advances in Chromatography*, 33, 1-66.

Meyer, V.R. (1985). High-Performance Liquid Chromotography Theory for the Practitioner, *J. Chromotography*, *197*, 334.

Paegel, Brian, M, Hutt, Lester D, Simpson, Peter C., & Mathies, Richard, A. (2000). Turn Geometry for Minimizing Band Broadening in Microfabricated Capillary Electrophoresis Channels, *Analytical Chemistry*, *72*, 3030-3037.

Probstein, Ronald, F. (1989). *Physicochemical Hydrodynamics: An Introduction.* Butterworth-Heinemann.

Tyrrell, H, & Harris, K. (1984). *Diffusion in Liquids: A Theoretical and Experimental Study*. Butterworth & Co.

Appendix: Sample Calculations

Calculation 1: Analytical Solution to Sample Travelling in One-Dimension, from Figure 22.

$$\phi = \frac{c - c_i}{c_1 - c_i} = \frac{1}{2}(erf(\frac{s-(x-vt)}{(2\sqrt{Dt}}) + erf(\frac{s+(x-vt)}{2\sqrt{Dt}}) = \frac{1}{2}(erf(\frac{s-(x+(\mu_{eo}+\mu_{ep})*\vec{E}*t)}{2\sqrt{Dt}}$$

$$+ erf(\frac{s+(x+(\mu_{eo}+\mu_{ep})*\vec{E}*t)}{2\sqrt{Dt}}) = \frac{1}{2}(erf(\frac{5E^{-5}-(2.7E^{-3}+(1E^{-8}+1E^{-9})*5E^{3}*45)}{2\sqrt{8.46E^{-10}*45}}$$

$$+ erf(\frac{5E^{-5}+(2.7E^{-3}+(1E^{-8}+1E^{-9})*5E^{3}*45)}{2\sqrt{8.46E^{-10}*45}}) = 0.132$$

Calculation 2: Dispersion in X-Direction and Mean of Cross-Section, from Figure 24, δ=1.96.

$$Dispersion = <x>_{upper} - <x>_{lower} = \frac{\sum x*C*\Delta x}{\sum C*\Delta x} - \frac{\sum x*C*\Delta x}{\sum C*\Delta x} =$$

$$\frac{\sum x*C*\Delta x}{\sum C*\Delta x} - \frac{\sum x*C*\Delta x}{\sum C*\Delta x} =$$

$$\frac{0*3.39E^{-24}*(1)+3.03E^{-5}*1.41E^{-24}*(1)+\ldots+2.54E^{-3}*3.45E^{-1}*(1)+\ldots+3E^{-3}*8.75E^{-8}*(1)}{3.39E^{-24}*(1)+1.41E^{-24}*(1)+\ldots+3.45E^{-1}*(1)+\ldots+8.75E^{-8}*(1)} -$$

$$\frac{0*1.27E^{-16}*(1)+3.03E^{-5}*2.06E^{-16}*(1)+\ldots+2.54E^{-3}*7.39E^{-24}*(1)+\ldots+3E^{-3}*1.46E^{-22}*(1)}{1.27E^{-16}*(1)+2.06E^{-16}*(1)+\ldots+7.39E^{-24}*(1)+\ldots+1.46E^{-22}*(1)} =$$

$$1.22E^{-3}$$

Calculation 3: Peclet Number, from Figure 24, δ=1.96.

$$Pe = \frac{Ua}{D} = \frac{\frac{V}{L}(\mu_{eo}(y)+\mu_{ep})a}{D} =$$

$$\frac{\frac{30-0}{.003*2+3.14*(.000002+.000177/2)}*(0+1.25E^{-8})*.000177}{0} =$$

$$+\infty \approx 510000$$

Calculation 4: Normalized Radius of Turn, from Figure 24.

$$\delta = \frac{\bar{r}}{a} = \frac{r + a/2}{a} = \frac{.000002 + \frac{.000177}{2}}{.000177} = 1.96$$

Calculation 5: Modified Peclet Number, from Figure 24.

$$\delta Pe = 1.96 * 510000 = 1E^{6}$$

Calculation 6: Rectangular Based Variance/Dispersion Variance.

Assuming a square concentration distribution with the mean of the concentration at 0, total width Δl, and concentration height c, the variance may be calculated in the following manner:

$$< x^2 >= \frac{\int (x - < x >)^2 c(x) dx}{\int c(x) dx} = \frac{\int_{-\frac{\Delta l}{2}}^{\frac{\Delta l}{2}} (x-0)^2 c dx}{\int_{-\frac{\Delta l}{2}}^{\frac{\Delta l}{2}} c dx} = \frac{\frac{x^3}{3} c}{xc} = \frac{\frac{\left(\frac{\Delta l}{2}\right)^3}{3} c + \frac{\left(\frac{\Delta l}{2}\right)^3}{3} c}{\Delta l c} = \frac{\Delta l^2}{12}$$

Calculation 7: Normalized Dispersion Variance, Figure 25.

$$\frac{< x^2 >}{a^2} = \frac{\frac{\Delta l^2}{12}}{a^2} = \frac{\frac{1.22E^{-3}}{12}}{.000177^2} = 3.93$$

Calculation 8: Normalized Dispersion from Griffiths and Nilson, Figure 25, δ=1.96

$$\left(\frac{\sigma}{a}\right)^2 = \frac{\theta^2 \delta Pe}{15\theta + 3\delta Pe} = \frac{3.14^2 * 1.96 * 510000}{15 * 3.14 + 3 * 1.96 * 510000} = 3.29$$

Calculation 9: Variance, Normalized Variance, Figure 27, δ=1.96

$$< x >= \frac{\sum x * (\sum_{y=0}^{a} C(x)_{across-channel}) * \Delta x}{\sum (\sum_{y=0}^{a} C(x)_{across-channel}) * \Delta x} =$$

$$\frac{(0 * 8.37E^{-18} * (1) + 3.03E^{-3} * 9.17E^{-18} * (1) + \ldots + 2.54E^{-3} * 7.52E^{-1} * (1) + \ldots + 3E^{-3} * 1.41E^{-2} * (1)}{8.37E^{-18} * (1) + 9.17E^{-18} * (1) + \ldots + 7.52E^{-1} * (1) + \ldots + 1.41E^{-2} * (1)} = .216$$

$$< x^2 >= \frac{\sum (x - < x >)^2 (\sum_{y=0}^{a} C(x)_{across-channel}) * \Delta x}{\sum (\sum_{y=0}^{a} C(x)_{across-channel}) * \Delta x} =$$

$$\frac{(0 - 1.73E^{-3})^2 * 8.37E^{-18} * (1) + (3.03E^{-5} - 1.73E^{-3})^2 * 9.17E^{-18} * (1) + \ldots}{8.37E^{-18} * (1) + 9.17E^{-18} * (1) + \ldots}$$

$$\frac{\ldots + (2.54E^{-3} - 1.73E^{-3})^2 * 7.52E^{-1} * (1) + \ldots + (3E^{-3} - 1.73E^{-3})^2 * 1.41E^{-2} * (1)}{\ldots + 7.52E^{-1} * (1) + \ldots + 1.41E^{-2} * (1)} = 1.36E^{-7}$$

$$\frac{< x^2 >}{a^2} = \frac{1.36E^{-7}}{0.000177^2} = 4.37$$

Calculation 10: Scaled Variance, Figure 28, δ=1.96.

$$\frac{< x^2 > -2Dt}{2\theta a^2} = \frac{1.36E - 7 - 2 * 0 * 72}{2 * 3.14 * 0.000177^2} = 1.11E^{-1}$$

Calculation 11: Time Ratio, Figure 28, δ=1.96.

$$\frac{t_d}{t_t} = \frac{a^2 v_c r_c}{2D\theta(r_c + a/2)^2} = \frac{a^2(\mu_{eo} + \mu_{ep})\frac{V}{r_c} r_c}{2D\theta(r_c + a/2)^2} = \frac{a^2(\mu_{eo} + \mu_{ep})V}{2D\theta(r_c + a/2)^2} =$$

$$\frac{0.000177^2 * (0 + 1.25E^{-8}) * 30}{2 * 0 * 3.14 * (2 * .003 + 3.14 * (2E^{-5} + \frac{1.77E^{-4}}{2}) + \frac{.000177}{2})^2} =$$

$$+\infty \approx 1000$$

Calculation 12: Plate Height to Dispersion, from Figure 29 to Figure 30, EO

Speed=0.85 cm/s

$$H = \frac{2D_{eff}}{u_{EO}}$$

$$D_{eff} = \frac{Hu_{eo}}{2}$$

$$w^2 = 13.139 D_{eff}(t - t_0) = 13.139 * \frac{Hu_{eo}}{2}(t - t_0)$$

$$t = \frac{estimated\ travel\ distance}{eo\ velocity} = \frac{.000500}{.0085} = .059$$

$$w = \sqrt{13.139 * \frac{Hu_{eo}}{2}(t - t_0)} = \sqrt{13.139 * \frac{0.0000027 * .0085}{2}(.059)} = .000094\ um$$

Calculation 13: Anticipated Dispersion Change, Figure 30, for All Speeds, Non-Modified Turn to Modified Turn, for 4 Percent Speed Ratio, and Modified Length of 500 μm.

$$v_{\mathrm{mod}} = 1.04 * v_{un\,\mathrm{mod}}$$

$$t = \frac{l_{un\,\mathrm{mod}}}{v_{un\,\mathrm{mod}}}$$

$$\Delta w_{\mathrm{mod}-un\,\mathrm{mod}} = v_{\mathrm{mod}} t - v_{un\,\mathrm{mod}} t = v_{\mathrm{mod}} \frac{l_{un\,\mathrm{mod}}}{v_{un\,\mathrm{mod}}} - v_{un\,\mathrm{mod}} \frac{l_{un\,\mathrm{mod}}}{v_{un\,\mathrm{mod}}} = 1.04 l_{un\,\mathrm{mod}} - l_{un\,\mathrm{mod}} = 0.04 * l_{un\,\mathrm{mod}} =$$

$$0.04 * l_{\mathrm{mod}} = 0.04 * 500um = 20um$$

Calculation 14: Percent Error of Expected Electroosmotic Flow Position from Simulated Electroosmotic Flow Position. Data from Figure 39, Speed Ratio of 3.00, Upper Edge of Channel.

$$predicted\ travel = (\mu_{eo} + \mu_{ep}) * \vec{E} * t = (1e^{-8} + 1e^{-9}) * \frac{30}{.0006} * 45 = 2.48e^{-3}$$

$$\%\ error = \frac{predicted - actual}{predicted} * 100 = \frac{2.48e^{-3} - 2.20e^{-3}}{2.48e^{-3}} = 12.2\%$$